Chinese Journal of
POLYMER SCIENCE

REVIEW

https://doi.org/10.1007/s10118-024-3197-2
Chinese J. Polym. Sci. **2024**, *42*, 1302–1312

Density-Functional Theories for Polyelectrolyte Systems

Jia-Wei Zhang[a], Yu-Hang Zhang[a], Bao-Hui Li[a*], and Qiang Wang[b*]

[a] *School of Physics, Nankai University, Tianjin 300071, China*
[b] *Department of Chemical and Biological Engineering, Colorado State University, 1370 Campus Delivery, Fort Collins, CO 80523-1370, USA*

Abstract Polymer density-functional theories (PDFTs) have distinct advantages in the study of polyelectrolyte (PE) systems over experiments and molecular simulations. Here we give an introductory review of some PDFTs recently developed for PE systems. We start with a general formalism of PDFTs and its relation to the widely used polymer self-consistent field theory (SCFT), then explain the various correlations that are neglected in SCFT but can be accounted for in PDFTs, including those due to the excluded-volume interaction and chain connectivity of uncharged polymers, the electrostatic correlations of small ions, and the chain correlations in PEs. We also list some applications of PDFTs for PE systems, and finally give some perspectives on future work. We hope that our review can attract more researchers to apply and further develop PDFTs as a promising class of theoretical and computational tools.

Keywords Polymer density-functional theories; Polyelectrolytes; Correlations

Citation: Zhang, J. W.; Zhang, Y. H.; Li, B. H.; Wang, Q. Density-functional theories for polyelectrolyte systems. *Chinese J. Polym. Sci.* **2024**, *42*, 1302–1312.

1 INTRODUCTION

Polyelectrolyte (PE) systems usually consist of many charged polymers (*e.g.*, polystyrene sulfonate, polyacrylic acid, DNA, RNA, and proteins) and ions in water, and are ubiquitous and indispensable in many industrial and biological processes. PEs include, for example, important biological molecules, materials used to deliver genes and vaccines, and molecules used as stabilizers in food and pharmaceuticals. The behavior of PEs governs the properties of biological fluids, the stability and safety of food and pharmaceuticals, and molecular recognition in biosensors, just to name a few. Despite their technological significance to many disciplines, however, PEs remain among the least understood polymers with many controversies due to the presence of both short-range (excluded-volume) and long-range (Coulomb) interactions in these systems. Experiments on PE systems are notoriously difficult to do due to the many more parameters that need to be well-controlled than uncharged polymeric systems. Full atomistic simulations of many-chain systems are currently not feasible due to their formidable computational requirements; even molecular simulations of coarse-grained PE systems are challenging due to the long-range nature of Coulomb interactions. While these problems encountered in experiments and molecular simulations can be handled in theories, classical mean-field theories of PE systems, such as the Poisson-Boltzmann and Derjaguin-Landau-Verwey-Overbeek theories, neglect several important factors including the system fluctuations/correlations, ion specificity, and dielectric mismatch between polymers and water (and confining surfaces, if present); they therefore cannot explain many fundamentally important but controversial phenomena observed in experiments (*e.g.*, the Hofmeister series, effects of multivalent ions, like-charge attractions).

Here we give an introductory review of some polymer density-functional theories (PDFTs) recently developed for PE systems, which belong to the classical DFT and are very promising to overcome some of the above issues in classical mean-field theories including the widely used polymer self-consistent field theory (SCFT).[1] The basic idea of DFT is that there exists a unique free-energy functional of the spatially varying particle number densities for a system under given external potentials, and the minimum value of this functional gives the equilibrium free energy of the system.[2,3] Our goal here is not to be exhaustive, but to introduce PDFTs for PE systems in a progressive way to researchers who are new to them. We start with a general formalism of PDFTs and its relation to SCFT (Sec. **2**), then explain the various correlations that can be accounted for in PDFTs, including those due to the excluded-volume interaction and chain connectivity of uncharged polymers (Sec. **3**) followed by the electrostatic correlations of small ions (Sec. **4**) and finally the chain correlations in PEs (Sec. **5**). We also list some applications of PDFTs for PE systems (Sec. **6**), before we give some perspectives on future work (Sec. **7**). We hope that our review can attract more researchers to apply and further develop PDFTs as a promising class of theoretical and computational tools.

* Corresponding authors, E-mail: baohui@nankai.edu.cn (B.H.L.)
E-mail: qwang@colostate.edu (Q.W.)

Special Issue: Charged Polymers
Received May 24, 2024; Accepted June 21, 2024; Published online August 8, 2024

Table 1 List of Symbols and Acronyms.

~	dimensionless	$\hat{f}$	Fourier transform of a radial function $f(r)$
Superscripts:			
B	bonded	C	Coulomb
CH	chain connectivity	ex	excess
id	ideal	S	shell
Subscripts:			
b	bulk	c	chain
i, j	species	r	reference
s, t	segment		
Symbols:			
$c(r)$	direct pair correlation function	$\delta(r)$	Dirac δ-function
e	elementary charge	ε	dielectric constant
ε_0	vacuum permittivity	ε_r	relative dielectric constant
f	Helmholtz free-energy density	F	Helmholtz free energy
$\Phi(\mathbf{r})$	local Helmholtz free-energy density	$g(\sigma)$	contact value of the radial distribution function
h	truncation distance	$h(r)$	total pair correlation function
k_B	Boltzmann constant	m	total number of molecular species
μ	chemical potential	$m_\alpha(\mathbf{r})$, $n_\alpha(\mathbf{r})$	weighted densities
N	chain length	$q(\mathbf{r})$	propagator
$\Theta(r)$	Heaviside step-function	$\mathbf{r}$, $\mathbf{R}$	spatial position
R	radius	ρ	number density
$s(\mathbf{r})$	local charge density	σ	hard-sphere diameter
T	thermodynamic temperature	u	internal-energy density
$u(r)$	non-bonded pair potential	U_c^B	bonded energy of a chain
v	excluded-volume parameter	V	volume
$V(\mathbf{r})$	external potential	$w_\alpha(r;R)$	scalar weight functions
$\mathbf{w}_\alpha(r;R)$	vector weight functions	Ω	grand potential
$y(\sigma)$	contact value of the cavity correlation function	$\psi(\mathbf{r})$	electrostatic potential
Z	valence		
Acronyms:			
BFD	bulk fluid density	BPE	block polyelectrolyte
CCF	cavity correlation function	CHS	charged hard sphere
CJ	Chang and Jiang	CKE	Chapman-Kolmogorov equation
CSM	charged-shell model	DFT	density-functional theory
EC	electrostatic correlation	ELE	Euler-Lagrange equation
EXP	exponential approximation	fCSM	full charged-shell model
fMSA	functionalized mean-spherical approximation	FMT	fundamental measure theory
HS	hard sphere	JGW	Jiang, Ginzburg and Wang
LW	Li and Wu	MC	Monte Carlo
MF	mean-field	mfMSA	modified functionalized mean-spherical approximation
mFMT	modified fundamental measure theory	MSA	mean-spherical approximation
OZ	Ornstein-Zernike	PCF	pair correlation function
PCM	point-charge model	PDFT	polymer density-functional theory
PE	polyelectrolyte	PY	Percus-Yevick
QJ	Qing and Jiang	RDF	radial distribution function
RFD	reference fluid density	SCFT	self-consistent field theory
tCSM	truncated charged-shell model	THSC	tangent hard-sphere chain
TPT	thermodynamic perturbation theory	TPT1	first-order thermodynamic perturbation theory

2 A GENERAL FORMALISM OF PDFTs OF PEs

PDFTs are usually formulated in a grand-canonical ensemble. For simplicity, let us consider a model PE system of m molecular species in volume V at thermodynamic temperature T and given chemical potential μ_i of species i (=1, …, m); the system is in a uniform medium of dielectric constant $\varepsilon \equiv 4\pi\varepsilon_0\varepsilon_r$, where $\varepsilon_0 \approx 8.854\times10^{-12}$ $A^2\cdot s^2\cdot J^{-1}\cdot m^{-1}$ is the vacuum permittivity and ε_r the relative dielectric constant of the medium (≈78.5 for water at T=298 K), and under the given external potentials $V_i(\mathbf{r})$ acting on each segment of species i at spatial position $\mathbf{r}$ due to, for example, the confinement of hard (impenetrable) surfaces. Unless specified otherwise, we treat species i as a (ungrafted) homopolymer of N_i segments each having diameter σ_i and carrying Z_i elementary charges e (≈1.602×10^{-19} A·s), with N_i=1 for small-molecule species (*e.g.*, ions) and Z_i=0 for uncharged species. Hereafter we take k_BT as the unit of energy with k_B being the Boltzmann constant, e as the unit of charge, and some segment diameter σ as the unit of length without loss of generality; all quantities used below are therefore dimensionless (*e.g.*, $\tilde{\sigma}_i \equiv \sigma_i/\sigma$, $\tilde{V} \equiv V/\sigma^3$, $\tilde{\mu}_i \equiv \mu_i/k_BT$, $\tilde{V}_i(\mathbf{r}) \equiv V_i(\mathbf{r})/k_BT$ and $\tilde{\varepsilon} \equiv \varepsilon k_BT\sigma/e^2$), unless noted otherwise.

The grand potential of our model system is given *via* the Legendre transform as $\Omega \equiv F^{id}[\{\rho_{c,i}\}] + F^{ex}[\{\rho_i\}] + \sum_i \int d\mathbf{R}_i$

https://doi.org/10.1007/s10118-024-3197-2

$\left(\sum_{s=1}^{N_i}\tilde{V}_i(\mathbf{R}_{s,i})-\tilde{\mu}_i\right)\rho_{c,i}(\mathbf{R}_i)$,[4] where $F^{\mathrm{id}}[\{\rho_{c,i}\}]=\sum_i\int d\mathbf{R}_i\rho_{c,i}(\mathbf{R}_i)\left(\ln\rho_{c,i}(\mathbf{R}_i)-1+U^{\mathrm{B}}_{c,i}(\mathbf{R}_i)\right)$ is the ***exact*** Helmholtz free energy of an ideal system (*i.e.*, same as the above model system but without non-bonded interactions) written as a functional of the (dimensionless) chain number density distribution $\rho_{c,i}(\mathbf{R}_i)$ of species i, $\mathbf{R}_i\equiv\{\mathbf{R}_{s,i}\}$ denotes a chain configuration of species i with $\mathbf{R}_{s,i}$ being the (dimensionless) spatial position of segment s (=1, … , N_i) on the chain and $\int d\mathbf{R}_i\equiv\prod_{s=1}^{N_i}\int d\mathbf{R}_{s,i}$, $U^{\mathrm{B}}_{c,i}$ is the bonded energy of a chain of species i (note that $U^{\mathrm{B}}_{c,i}=0$ for small-molecule species), and $F^{\mathrm{ex}}[\{\rho_i\}]$ is the ***approximate*** excess Helmholtz free energy of the above model system due to its non-bonded interactions written as a functional of the total segment number density profile $\rho_i(\mathbf{r})\equiv\sum_{s=1}^{N_i}\rho_{s,i}(\mathbf{r})$ of species i with $\rho_{s,i}(\mathbf{r})\equiv\int d\mathbf{R}_i\rho_{c,i}(\mathbf{R}_i)\delta(\mathbf{r}-\mathbf{R}_{s,i})$. Setting the functional derivatives $\delta\Omega/\delta\rho_{c,i}(\mathbf{R}_i)=0$ then gives the Euler-Lagrange equations (ELEs) for the equilibrium segment number density profiles

$$\rho_{s,i}(\mathbf{r})=\exp(\tilde{\mu}_i)\int d\mathbf{R}_i\exp\left(-U^{\mathrm{B}}_{c,i}(\mathbf{R}_i)-\sum_{s=1}^{N_i}\lambda_i(\mathbf{R}_{s,i})\right)\delta(\mathbf{r}-\mathbf{R}_{s,i}) \quad (1)$$

with $\lambda_i(\mathbf{r})\equiv\delta F^{\mathrm{ex}}/\delta\rho_i(\mathbf{r})+\tilde{V}_i(\mathbf{r})$ for all s and i, which minimize Ω; note that we have used $\delta F^{\mathrm{ex}}/\delta\rho_{c,i}(\mathbf{R}_i)=\sum_{s=1}^{N_i}\delta F^{\mathrm{ex}}/\delta\rho_i(\mathbf{R}_{s,i})$ to obtain the above equation.

2.1 Relation to SCFT

With $u_{ij}(r)$ denoting the (isotropic) non-bonded pair potential between segments of species i and j, the simplest approximation for F^{ex}, known as the mean-field approximation,[5] is given by $F^{\mathrm{MF}}[\{\rho_i\}]=\int d\mathbf{r}d\mathbf{r}'\sum_i\sum_j\rho_i(\mathbf{r})u_{ij}(|\mathbf{r}-\mathbf{r}'|)\rho_j(\mathbf{r}')/2$; substituting it into Eq. (1) leads to the widely used SCFT[1], which neglects the system correlations/fluctuations. This can be easily seen in the case of flexible chains, where $U^{\mathrm{B}}_{c,i}(\mathbf{R}_i)=\sum_{s=1}^{N_i-1}u^{\mathrm{B}}_i(|\mathbf{R}_{s+1,i}-\mathbf{R}_{s,i}|)$ with $u^{\mathrm{B}}_i(r)$ denoting the normalized (*i.e.*, $\int d\mathbf{r}\exp\left(-u^{\mathrm{B}}_i(|\mathbf{r}|)\right)=1$) bonding potential between two adjacent segments on a chain of species i and Eq. (1) becomes:

$$\rho_{s,i}(\mathbf{r})=\exp(\tilde{\mu}_i)\prod_{t=1}^{s-1}\int d\mathbf{R}_{t,i}\cdot\exp\left(-\sum_{t=1}^{s-2}u^{\mathrm{B}}_i(|\mathbf{R}_{t+1,i}-\mathbf{R}_{t,i}|)-\sum_{t=1}^{s-1}\lambda_i(\mathbf{R}_{t,i})\right)\cdot\int d\mathbf{R}_{s,i}\delta(\mathbf{r}-\mathbf{R}_{s,i})\exp\left(-u^{\mathrm{B}}_i(|\mathbf{R}_{s,i}-\mathbf{R}_{s-1,i}|)-\lambda_i(\mathbf{R}_{s,i})\right)\cdot\prod_{t=s+1}^{N_i}\int d\mathbf{R}_{t,i}\cdot\exp\left(-u^{\mathrm{B}}_i(|\mathbf{R}_{s+1,i}-\mathbf{R}_{s,i}|)-\sum_{t=s+1}^{N_i-1}u^{\mathrm{B}}_i(|\mathbf{R}_{t+1,i}-\mathbf{R}_{t,i}|)-\sum_{t=s+1}^{N_i}\lambda_i(\mathbf{R}_{t,i})\right)$$

with $\lambda_i(\mathbf{r})=\lambda^{\mathrm{SCFT}}_i(\mathbf{r})=\int d\mathbf{r}'\sum_j u_{ij}(|\mathbf{r}-\mathbf{r}'|)\rho_j(\mathbf{r}')+\tilde{V}_i(\mathbf{r})$ and the "·" indicating that the products before it do not apply to the terms after it (but the integrals do); defining the one-end-integrated forward propagator (as commonly used in SCFT) $q_{s,i}(\mathbf{r})\equiv\exp(-\lambda_i(\mathbf{r}))\prod_{t=1}^{s-1}\int d\mathbf{R}_{t,i}\cdot\exp(-u^{\mathrm{B}}_i(|\mathbf{r}-\mathbf{R}_{s-1,i}|)-\sum_{t=1}^{s-2}u^{\mathrm{B}}_i(|\mathbf{R}_{t+1,i}-\mathbf{R}_{t,i}|)-\sum_{t=1}^{s-1}\lambda_i(\mathbf{R}_{t,i}))$ of species i, which corresponds to the probability of finding a partial chain of s segments of species i that ends at $\mathbf{r}$ and satisfies the Chapman-Kolmogorov equation (CKE) $q_{s,i}(\mathbf{r})=\exp(-\lambda_i(\mathbf{r}))\int d\mathbf{r}'\exp\left(-u^{\mathrm{B}}_i(|\mathbf{r}-\mathbf{r}'|)\right)q_{s-1,i}(\mathbf{r}')$ for s=2, …, N_i with $q_{1,i}(\mathbf{r})=\exp(-\lambda_i(\mathbf{r}))$, and similarly the backward propagator $q^{\dagger}_{s,i}(\mathbf{r})\equiv\exp(-\lambda_i(\mathbf{r}))\prod_{t=s+1}^{N_i}\int d\mathbf{R}_{t,i}\cdot\exp\left(-u^{\mathrm{B}}_i(|\mathbf{R}_{s+1,i}-\mathbf{r}|)-\sum_{t=s+1}^{N_i-1}u^{\mathrm{B}}_i(|\mathbf{R}_{t+1,i}-\mathbf{R}_{t,i}|)-\sum_{t=s+1}^{N_i}\lambda_i(\mathbf{R}_{t,i})\right)$, which for homopolymers is just $q_{N_i-s+1,i}(\mathbf{r})$, we obtain $\rho_{s,i}(\mathbf{r})=\exp(\tilde{\mu}_i+\lambda_i(\mathbf{r}))q_{s,i}(\mathbf{r})q^{\dagger}_{s,i}(\mathbf{r})$ (for small-molecule species this becomes $\rho_i(\mathbf{r})=\exp(\tilde{\mu}_i-\lambda_i(\mathbf{r}))$). Note that the propagators defined here are slightly different from the q-functions used in Ref. [6] or the G-functions in Ref. [7], but the same as the G-functions in Ref. [8].

As recently noted by one of us, for systems with short-range $u_{ij}(r)$ SCFT can only be applied to soft-core models, where $\int d\mathbf{r}u_{ij}(|\mathbf{r}|)$ is finite (for all ij-pairs) and one can define the excluded-volume parameters $v_{ij}>0$ *via* $u_{ij}(r)=v_{ij}u_{0,ij}(r)$ with the normalized non-bonded pair potentials $u_{0,ij}(r)$ satisfying $\int d\mathbf{r}u_{0,ij}(|\mathbf{r}|)=1$; in the limit of the number of chains $n_i\to\infty$ (for all species i), with $v_{ij}\propto\rho^{-1}$ and $\rho\equiv\sum_i n_iN_i\sigma^3/V$ denoting the total segment number density in the system (in a canonical ensemble), the mean-field approximation inherent in SCFT becomes exact and there are neither fluctuations (which are due to the presence of different energy levels) nor correlations (which are due to the finite non-bonded interactions) in the system.[9,10] The various correlations neglected by SCFT, however, can be accounted for in PDFTs, as shown in Secs. **3**–**5** below.

2.2 On the Mean-Field Contribution due to the Coulomb Interaction

Taking the Coulomb potential $u^{\mathrm{C}}(r)=1/\tilde{\varepsilon}r$ between two (point) elementary charges separated at a distance r as an example (*i.e.*, with $u_{ij}(r)=Z_iZ_ju^{\mathrm{C}}(r)$), while $\int d\mathbf{r}u^{\mathrm{C}}(|\mathbf{r}|)$ diverges, the (long-range) Coulomb interaction can be treated in SCFT by introducing the mean-field electrostatic potential $\psi(\mathbf{r})$ satisfying the Poisson equation $\tilde{\varepsilon}\nabla^2\psi(\mathbf{r})=-4\pi\sum_i Z_i\rho_i(\mathbf{r})$ with appropriate boundary conditions. The mean-field contribution to F^{ex} due to the Coulomb interaction, F^{MF}, of this point-charge model (PCM) is then given by $F^{\mathrm{MF}}_{\mathrm{PCM}}[\{\rho_i\}]=\int d\mathbf{r}\psi(\mathbf{r})\sum_i Z_i\rho_i(\mathbf{r})$. Alternatively, one can use the mean-field approximation to write $F^{\mathrm{MF}}_{\mathrm{PCM}}[\{\rho_i\}]=\int d\mathbf{r}d\mathbf{r}'\sum_i\sum_j Z_iZ_j\rho_i(\mathbf{r})u^{\mathrm{C}}(|\mathbf{r}-\mathbf{r}'|)\rho_j(\mathbf{r}')/2$. With $\int d\mathbf{r}d\mathbf{r}'\sum_i\sum_j Z_iZ_j\rho_i(\mathbf{r})u^{\mathrm{C}}(|\mathbf{r}-\mathbf{r}'|)\rho_j(\mathbf{r}')/2=\int d\mathbf{r}\sum_i Z_i\rho_i(\mathbf{r})\psi(\mathbf{r})/2=(\tilde{\varepsilon}/8\pi)\int d\mathbf{r}|\nabla\psi(\mathbf{r})|^2$, where $\psi(\mathbf{r})\equiv\int d\mathbf{r}'\sum_j Z_ju^{\mathrm{C}}(|\mathbf{r}-\mathbf{r}'|)\rho_j(\mathbf{r}')$ is the electrostatic potential, one can re-write $F^{\mathrm{MF}}_{\mathrm{PCM}}$ also as a functional of $\psi(\mathbf{r})$, *i.e.*, $F^{\mathrm{MF}}_{\mathrm{PCM}}[\{\rho_i\},\psi]=\int d\mathbf{r}\left[\psi(\mathbf{r})\sum_i Z_i\rho_i(\mathbf{r})-(\tilde{\varepsilon}/8\pi)|\nabla\psi(\mathbf{r})|^2\right]$; setting $\delta F^{\mathrm{MF}}_{\mathrm{PCM}}/\delta\psi(\mathbf{r})=0$ then gives the Poisson equation.[11,12]

For the reason given at the end of Sec. **4.1** below, Gillespie and co-workers[13–17] used the charged-shell model (CSM)[18] for F^{MF}, where the charges carried by an ion of species i at, without loss of generality, $\mathbf{r}_i$=(0,0,0) are evenly distributed on a spherical shell of radius R_i (which may not be $\tilde{\sigma}_i/2$) centered at $\mathbf{r}_i$; its local charge density is therefore given by

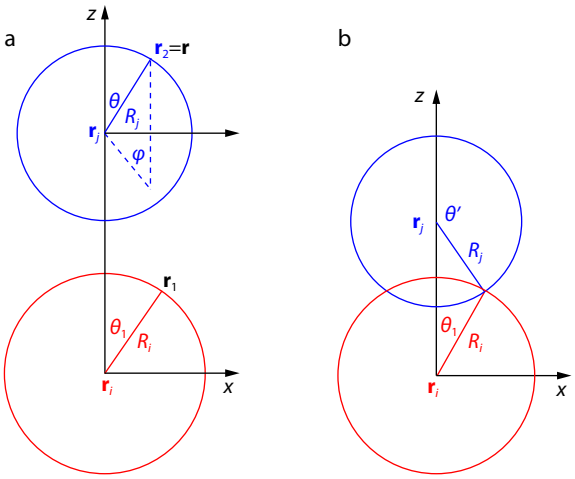

Fig. 1 Schematics for the charged-shell model, where two ions of species *i* and *j* having the charged-shell radii R_i and R_j, respectively, are located at $\mathbf{r}_i$ and $\mathbf{r}_j$. $|\mathbf{r}_i - \mathbf{r}_j| > R_i + R_j$ in (a) and $R_i + R_j > |\mathbf{r}_i - \mathbf{r}_j| > R_i - R_j$ in (b). See the main text for more details.

$s_i(\mathbf{r}) = \left(Z_i/4\pi R_i^2\right)\delta\left(|\mathbf{r}| - R_i\right)$, and the electrostatic potential at $\mathbf{r}$ generated by this ion, $\psi_i(\mathbf{r})$, depends only on $r \equiv |\mathbf{r}|$ due to the spherical symmetry. Without loss of generality, we can take $\mathbf{r}=(0,0,r)$ and obtain $\psi_i(\mathbf{r}) = \int d\mathbf{r}_1 s_i(\mathbf{r}_1)/\tilde{\varepsilon}|\mathbf{r} - \mathbf{r}_1|$; integrating over $\mathbf{r}_1 = (r_1,\theta_1,\varphi_1)$ in the spherical coordinates shown in Fig. 1(a) then gives $\psi_i(\mathbf{r}) = Z_i/\tilde{\varepsilon}\max(r, R_i)$. As expected, $\psi_i(\mathbf{r})$ is constant inside the shell, and is the same as that generated by a point charge Z_i at $\mathbf{r}_i$ outside the shell. Similarly, the charges carried by an ion of species *j* at $\mathbf{r}_j$ are evenly distributed on a spherical shell of radius R_j with its local charge density being $s_j(\mathbf{r}) = \left(Z_j/4\pi R_j^2\right)\delta\left(|\mathbf{r} - \mathbf{r}_j| - R_j\right)$. Without loss of generality, we take $R_i \geq R_j$, $\mathbf{r}_j=(0,0,r_{ij})$ with $r_{ij} \equiv |\mathbf{r}_i - \mathbf{r}_j|$, and $\mathbf{r} = (R_j\sin\theta\cos\varphi, R_j\sin\theta\sin\varphi, r_{ij}+R_j\cos\theta)$; the pair potential between these two ions due to their Coulomb interaction is therefore given by $u_{ij}^S(r_{ij}) = \int d\mathbf{r} s_j(\mathbf{r})\psi_i(\mathbf{r})$. Since the integral over $\mathbf{r}$ is equivalent to that over $\mathbf{r}_2=(r_2,\theta,\varphi)$ in the spherical coordinates originated at $\mathbf{r}_j$ as shown in Fig. 1(a), we finally obtain $u_{ij}^S(r_{ij}) = Z_iZ_j/\tilde{\varepsilon}r_{ij}$ if $r_{ij} > R_i + R_j$, $u_{ij}^S(r_{ij}) = Z_iZ_j/\tilde{\varepsilon}R_i$ if $r_{ij} < R_i - R_j$, and $u_{ij}^S(r_{ij}) = \frac{Z_iZ_j}{2\tilde{\varepsilon}}\left(\int_{-1}^{t'} dt\frac{1}{R_i} + \int_{t'}^{1} dt\frac{1}{\sqrt{r_{ij}^2 + R_j^2 + 2r_{ij}R_jt}}\right) = \frac{Z_iZ_j\left[2r_{ij}\left(R_i + R_j\right) - \left(R_i - R_j\right)^2 - r_{ij}^2\right]}{4\tilde{\varepsilon}R_iR_jr_{ij}}$ otherwise with $t' \equiv \cos\theta' = \left(R_i^2 - R_j^2 - r_{ij}^2\right)/2r_{ij}R_j$ as shown in Fig. 1(b). The same results were recently obtained by Jiang and Gillespie,[17] who pointed out that the case of $r_{ij} < R_i - R_j$ was missed in Refs. [13–16]. They then re-wrote $F_{CSM}^{MF}[\{\rho_i\}] = \int d\mathbf{r}d\mathbf{r}' \sum_i\sum_j \rho_i(\mathbf{r})u_{ij}^S(|\mathbf{r} - \mathbf{r}'|)\rho_j(\mathbf{r}')/2$ as $F_{CSM}^{MF}[\{\rho_i\}, \psi] = \int d\mathbf{r}d\mathbf{r}' \sum_i\sum_j \rho_i(\mathbf{r})\Delta u_{ij}(|\mathbf{r} - \mathbf{r}'|)\rho_j(\mathbf{r}')/2 + F_{PCM}^{MF}[\{\rho_i\}, \psi]$ with $\Delta u_{ij}(r) \equiv u_{ij}^S(r) - Z_iZ_ju^C(r)$, and further introduced the truncation distances h_i and h_j for ions of species *i* and *j*, respectively, such that $\Delta u_{ij}(r)=0$ if $r > h_i + h_j$, $\left(Z_iZ_j/\tilde{\varepsilon}\right)\left(1/R_i - 1/r\right)$ if $r < R_i - R_j$, and $-Z_iZ_j\left(r - R_i - R_j\right)^2/4\tilde{\varepsilon}R_iR_jr$ otherwise; they referred to this as the full charged-shell model (fCSM) when $h_i = R_i$ for all *i*, and the truncated charged-shell model (tCSM) otherwise.[17] To be more specific, $h_i = \tilde{\sigma}_i/2 < R_i$ for all *i* is used in tCSM hereafter.

3 CORRELATIONS FOR UNCHARGED POLYMERS (THSCs)

As noted at the end of Sec. **2.1**, the various correlations neglected by SCFT can be accounted for in PDFTs. In particular, most PDFTs for PEs are based on that of Yu and Wu[7,19] for uncharged tangent hard-sphere chains (THSCs),[4] which uses Rosenfeld's fundamental measure theory (FMT)[20] or one of its improved versions (modified fundamental measure theories, mFMTs)[21,22] to account for the correlations due to the excluded-volume interaction in (inhomogeneous) HS mixtures and Wertheim's first-order thermodynamic perturbation theory (TPT1)[23] extended to inhomogeneous systems[7,24] to account for the correlations due to the chain connectivity; beyond the HS interaction, (short-range) interaction potentials such as the square-well, Yukawa, or Lennard-Jones potentials are usually treated with the mean-field approximation.[5]

For an inhomogeneous mixture of uncharged HSs (*i.e.*, Z_i=0 and N_i=1 for all *i*), FMT[20] or mFMT[21,22,25,26] gives its excess Helmholtz free energy due to the HS interaction as $F^{HS} = \int d\mathbf{r}\Phi^{HS}(\mathbf{r})$, where $\Phi^{HS}(\mathbf{r})$ is the corresponding local excess Helmholtz free-energy density at $\mathbf{r}$ and written as a ***function*** of three independent weighted densities: $\tilde{n}_2(\mathbf{r}) \equiv \sum_i \tilde{n}_{2,i}(\mathbf{r})$ with $\tilde{n}_{2,i}(\mathbf{r}) \equiv \int d\mathbf{r}'\rho_i(\mathbf{r}')\tilde{w}_2(|\mathbf{r} - \mathbf{r}'|; \tilde{\sigma}_i/2)$, $n_3(\mathbf{r}) \equiv \sum_i \int d\mathbf{r}'\rho_i(\mathbf{r}')w_3(|\mathbf{r} - \mathbf{r}'|; \tilde{\sigma}_i/2)$, and $\tilde{\mathbf{n}}_2(\mathbf{r}) \equiv \sum_i \tilde{\mathbf{n}}_{2,i}(\mathbf{r})$ with $\tilde{\mathbf{n}}_{2,i}(\mathbf{r}) \equiv \int d\mathbf{r}'\rho_i(\mathbf{r}')\tilde{\mathbf{w}}_2(\mathbf{r} - \mathbf{r}'; \tilde{\sigma}_i/2)$; here $\tilde{w}_2(r; R) = \delta(r - R)$ and $w_3(r; R) = \Theta(R - r)$ are scalar weight functions, $\tilde{\mathbf{w}}_2(\mathbf{r}; R) = -\nabla w_3(|\mathbf{r}|; R) = \delta(|\mathbf{r}| - R)\mathbf{r}/|\mathbf{r}|$ is a vector weight function, and $\Theta(x\geq 0)$=1 and 0 otherwise is the Heaviside step-function (note that six ***dimensional*** weighted densities are used Refs. [20–22,25–26]: $n_\alpha(\mathbf{r}) \equiv \sum_i n_{\alpha,i}(\mathbf{r})$ for α=0,1,2,3 and $\mathbf{n}_\alpha(\mathbf{r}) \equiv \sum_i \mathbf{n}_{\alpha,i}(\mathbf{r})$ for α=1,2 with $n_{2,i}(\mathbf{r}) = \tilde{n}_{2,i}(\mathbf{r})/\sigma$, $n_{0,i}(\mathbf{r}) = n_{2,i}(\mathbf{r})/\pi\sigma_i^2$, $n_{1,i}(\mathbf{r}) = n_{2,i}(\mathbf{r})/2\pi\sigma_i$, $\mathbf{n}_{2,i}(\mathbf{r}) = \tilde{\mathbf{n}}_{2,i}(\mathbf{r})/\sigma$ and $\mathbf{n}_{1,i}(\mathbf{r}) = \mathbf{n}_{2,i}(\mathbf{r})/2\pi\sigma_i$; for a bulk (*i.e.*, infinitely large and homogeneous, denoted by a subscript "*b*") system where $\rho_i(\mathbf{r}) = \rho_{i,b}$ for all *i* (here these are segment number densities having the dimension of $1/V$), one obtains $n_{0,i}(\mathbf{r})=\rho_{i,b}$, $n_{1,i}(\mathbf{r}) = \rho_{i,b}\sigma_i/2$, $n_{2,i}(\mathbf{r}) = \pi\rho_{i,b}\sigma_i^2$, $n_{3,i}(\mathbf{r}) = (\pi/6)\rho_{i,b}\sigma_i^3$, and $\mathbf{n}_{\alpha,i}(\mathbf{r})=\mathbf{0}$ for α=1,2). FMT gives $\Phi_{FMT}^{HS}(\mathbf{r}) = \left[-\tilde{n}_2(\mathbf{r})\ln\left(1-n_3(\mathbf{r})\right) + \tilde{n}_2^2(\mathbf{r})\zeta(\mathbf{r})/2\left(1-n_3(\mathbf{r})\right) + \tilde{n}_2^3(\mathbf{r})\left(3\zeta(\mathbf{r})-2\right)/24\left(1-n_3(\mathbf{r})\right)^2\right]/\pi$ with $\zeta(\mathbf{r}) \equiv 1 - \tilde{\mathbf{n}}_2(\mathbf{r}) \bullet \tilde{\mathbf{n}}_2(\mathbf{r})/\tilde{n}_2^2(\mathbf{r})$, which for a bulk system becomes the same as the excess Helmholtz free-energy density given by the scaled-particle theory, as well as the Ornstein-Zernike (OZ) equation with the Percus-Yevick closure (referred to as the PY theory) *via* the compressibility route, for HSs.[20] The most commonly used (but not the most accurate) mFMT gives $\Phi_{mFMT}^{HS}(\mathbf{r}) = \left[-\tilde{n}_2(\mathbf{r})\ln\left(1 - n_3(\mathbf{r})\right) + \tilde{n}_2^2(\mathbf{r})\zeta(\mathbf{r})/2\left(1 - n_3(\mathbf{r})\right) + v(\mathbf{r})\left(3\zeta(\mathbf{r}) - 2\right)/36\right]/\pi$ with $v(\mathbf{r}) \equiv \left(\tilde{n}_2^3(\mathbf{r})/n_3(\mathbf{r})\right)\left[1/\left(1 - n_3(\mathbf{r})\right) + \ln\left(1 - n_3(\mathbf{r})\right)/n_3(\mathbf{r})\right]$ (thus $F_{mFMT}^{HS} = \int d\mathbf{r}\Phi_{mFMT}^{HS}(\mathbf{r})$), which gives the Boublik-Mansoori-Carnahan-Starling-Leland equation of state[27,28] for a bulk system of HSs and has

been proven to be rather accurate (with only a few percent deviation from Monte Carlo, MC, results) for both one-component HS systems and HS mixtures over the entire range of densities.[21,22] We refer readers to Ref. [26] for a review on FMT and various mFMTs.

On the other hand, Wertheim's TPT[23] is for homogeneous polymeric systems and the case where an attractive site on a segment can take part in only one attractive interaction (*e.g.*, bond), known as the singly-bonded condition; segments each having one attractive site can only form dimers, those each having two attractive sites can form linear and ring polymers, and additional attractive sites allow the formation of branched polymers. The only approximation in TPT is the single-chain approximation, which considers only one chain in the system of monomeric segments. We refer readers to Ref. [29] for a pedagogical review on TPT.

For a bulk system of THSCs, Wertheim's TPT1 gives its excess Helmholtz free-energy density due to the chain connectivity

$$f^{\mathrm{CH}} = \sum_i \left(\frac{1}{N_i} - 1\right) \rho_{i,b} \ln y_{ii}(\tilde{\sigma}_i) \tag{2}$$

where $y_{ii}(\tilde{\sigma}_i)$ is the contact value of the cavity correlation function (CCF) between monomeric segments of species i; for an uncharged HS mixture, $y_{ii}(\tilde{\sigma}_i) = g_{ii}(\tilde{\sigma}_i)$, the contact value of the radial distribution function (RDF) between HSs of species i in the mixture. Note that because TPT1 only considers the bonding between a single pair of attractive sites, it conveys little information on chain architecture and cannot accurately predict the behavior of long-chain and low-density systems.[23] Yu and Wu used $g_{ii}(\tilde{\sigma}_i) = g_{ii}^{\mathrm{PY}}(\tilde{\sigma}_i) + \tilde{\sigma}_i^2 \tilde{\xi}_2^2 \big/ 72(1-\xi_3)^3$ given by the Boublik-Mansoori-Carnahan-Starling-Leland equation of state,[27,28] where $g_{ii}^{\mathrm{PY}}(\tilde{\sigma}_i) = 1/(1-\xi_3) + \tilde{\sigma}_i \tilde{\xi}_2 \big/ 4(1-\xi_3)^2$ is given by the PY theory with $\tilde{\xi}_2 \equiv \pi \sum_j \rho_{j,b} \tilde{\sigma}_j^2$ and $\xi_3 \equiv (\pi/6) \sum_j \rho_{j,b} \tilde{\sigma}_j^3$, and extended TPT1 to inhomogeneous (uncharged) THSCs by writing the excess Helmholtz free energy due to the chain connectivity as $F^{\mathrm{CH}} = \int \mathrm{d}\mathbf{r} \Phi^{\mathrm{CH}}(\mathbf{r})$ with the corresponding local excess Helmholtz free-energy density $\Phi^{\mathrm{CH}}(\mathbf{r})$ obtained from the above f^{CH} by replacing $\rho_{i,b}$, $\tilde{\xi}_2$, $\tilde{\xi}_2^2$ and ξ_3 with $\zeta_i(\mathbf{r})\tilde{n}_{2,i}(\mathbf{r})/\pi\tilde{\sigma}_i^2$, $\zeta(\mathbf{r})\tilde{n}_2(\mathbf{r})$, $\zeta(\mathbf{r})\tilde{n}_2^2(\mathbf{r})$ and $n_3(\mathbf{r})$, respectively, where $\zeta_i(\mathbf{r}) \equiv 1 - \tilde{\mathbf{n}}_{2,i}(\mathbf{r}) \bullet \tilde{\mathbf{n}}_{2,i}(\mathbf{r}) / \tilde{n}_{2,i}{}^2(\mathbf{r})$; this gives[7,24]

$$\Phi^{\mathrm{CH}}(\mathbf{r}) = \sum_i \frac{\zeta_i(\mathbf{r})\tilde{n}_{2,i}(\mathbf{r})}{\pi\tilde{\sigma}_i^2} \left(\frac{1}{N_i} - 1\right) \ln\left[\frac{1}{1-n_3(\mathbf{r})} + \frac{\tilde{\sigma}_i \zeta(\mathbf{r})\tilde{n}_2(\mathbf{r})}{4(1-n_3(\mathbf{r}))^2} + \frac{\tilde{\sigma}_i^2 \zeta(\mathbf{r})\tilde{n}_2^2(\mathbf{r})}{72(1-n_3(\mathbf{r}))^3}\right] \tag{3}$$

They compared the inter- and intrachain segment RDFs of uncharged THSCs each having $N \leq 20$ segments predicted by their PDFT with $F^{\mathrm{ex}} = F_{\mathrm{mFMT}}^{\mathrm{HS}} + F^{\mathrm{CH}}$ to those obtained from MC simulations and found good agreement.[19]

4 ELECTROSTATIC CORRELATIONS FOR ELECTROLYTES (CHSs)

4.1 Bulk Systems—The MSA Theory

Here we consider a bulk system of ions (*i.e.*, N_i=1 for all i) modeled as HSs with their charges located at the center of the sphere (*i.e.*, PCM, also referred to as charged hard spheres, CHSs, hereafter) under the electroneutrality condition, $\sum_i Z_i \rho_{i,b} = 0$. The OZ equation with the mean-spherical approximation closure (referred to as the MSA theory) then gives analytical results of the excess Helmholtz free energy due to the electrostatic correlations, F^{EC}, and the thermodynamic and structural properties of the system as shown below, which are used as the basis for PDFTs of PEs described in subsequent sections.

The OZ equation gives $\hat{h}_{ij}(q) = \hat{c}_{ij}(q) + \sum_k \rho_{k,b} \hat{c}_{ik}(q) \hat{h}_{kj}(q)$, where $h_{ij}(r)$ and $c_{ij}(r)$ are, respectively, the total and direct pair correlation functions (PCFs) between ions of species i and j in the system, and $\hat{f}(q) \equiv (4\pi/q) \int_0^\infty \mathrm{d}r r f(r) \sin(qr)$ is the 3D Fourier transform of a radial function $f(r)$ with q being the wavenumber. The MSA closure combines the exact result of $h_{ij}(r) = -1$ for $r < (\tilde{\sigma}_i + \tilde{\sigma}_j)/2$ and the approximation of $c_{ij}(r) = -Z_i Z_j u^{\mathrm{C}}(r)$ for $r \geq (\tilde{\sigma}_i + \tilde{\sigma}_j)/2$. Based on the factorization method of Baxter for mixtures,[30] Blum analytically solved the MSA theory for the general case of arbitrary charge and size in 1975;[31] the solution contains a single parameter $\tilde{\Gamma}_b$ obtained from[31–33]

$$\tilde{\Gamma}_b^2 = \frac{\pi}{\tilde{\varepsilon}} \sum_i \rho_{i,b} {X_{i,b}}^2 \tag{4}$$

with

$$X_{i,b} \equiv \frac{Z_i - \tilde{\eta}_b \tilde{\sigma}_i^2}{1 + \tilde{\Gamma}_b \tilde{\sigma}_i} \tag{5}$$

and

$$\tilde{\eta}_b \equiv \sum_i \frac{Z_i \rho_{i,b} \tilde{\sigma}_i}{1 + \tilde{\Gamma}_b \tilde{\sigma}_i} \Bigg/ \left[\frac{2}{\pi} + \frac{1}{3} \sum_i \frac{\rho_{i,b} \tilde{\sigma}_i^3 (2 - \tilde{\Gamma}_b \tilde{\sigma}_i)}{1 + \tilde{\Gamma}_b \tilde{\sigma}_i}\right] \tag{6}$$

He then obtained the internal-energy density due to the electrostatic correlations $u_b^{\mathrm{EC}} = -(1/\tilde{\varepsilon}) \sum_i \rho_{i,b} Z_i (Z_i - X_{i,b}) / \tilde{\sigma}_i$, the corresponding excess Helmholtz free-energy density $f_b^{\mathrm{EC}} = \int_0^{1/\tilde{\varepsilon}} d\lambda u_b^{\mathrm{EC}}(\lambda) / \lambda = \tilde{\Gamma}_b^3 \big/ 3\pi - (1/\tilde{\varepsilon}) \sum_i \rho_{i,b} Z_i (Z_i - X_{i,b}) / \tilde{\sigma}_i$ with $u_b^{\mathrm{EC}}(\lambda) = -\lambda \sum_i \rho_{i,b} Z_i (Z_i - X_{i,b}) / \tilde{\sigma}_i$ *via* the Kirkwood's charging process, and the corresponding excess chemical potential $\mu_{i,b}^{\mathrm{EC}} \equiv \left(\partial f_b^{\mathrm{EC}} / \partial \rho_{i,b}\right)_V = -\left\{\tilde{\Gamma}_b {Z_i}^2 / \left(1 + \tilde{\Gamma}_b \tilde{\sigma}_i\right) + \tilde{\eta}_b \tilde{\sigma}_i \left[\left(2Z_i - \tilde{\eta}_b \tilde{\sigma}_i^2\right) / \left(1 + \tilde{\Gamma}_b \tilde{\sigma}_i\right) + \tilde{\eta}_b \tilde{\sigma}_i^2 / 3\right]\right\} / \tilde{\varepsilon}$ of species i.[34] Based on Ref. [31], Hiroike obtained analytical results of the contact value of the RDF between CHSs of species i and j in the mixture

$$g_{ij}^{\mathrm{MSA}}\left(\left(\tilde{\sigma}_i + \tilde{\sigma}_j\right)/2\right) = g_{ij}^{\mathrm{PY}}\left(\left(\tilde{\sigma}_i + \tilde{\sigma}_j\right)/2\right) - \frac{2X_{i,b}X_{j,b}}{\tilde{\varepsilon}\left(\tilde{\sigma}_i + \tilde{\sigma}_j\right)} \tag{7}$$

where $g_{ij}^{\mathrm{PY}}((\tilde{\sigma}_i + \tilde{\sigma}_j)/2) = 1/(1-\xi_3) + \tilde{\xi}_2 \tilde{\sigma}_i \tilde{\sigma}_j / 2(1-\xi_3)^2 (\tilde{\sigma}_i + \tilde{\sigma}_j)$ is the corresponding value for uncharged HSs given by the PY theory, and their direct PCF $c_{ij}(r)$.[32]

Later, Wei and Blum pointed out that the above u_b^{EC} can be approximated (under the assumption of $\tilde{\eta}_b = 0$) by that in a mixture of charged spherical shells (thus CSM) of radius $R_i = \tilde{\sigma}_i / 2 + 1 / 2\tilde{\Gamma}_b$ for species i.[18] Blum and Rosenfeld further pointed out that $c_{ij}(r) - c_{ij}^{\mathrm{PY}}(r)$, where $c_{ij}^{\mathrm{PY}}(r)$ is the corresponding direct PCF for uncharged HS mixtures given by the PY theory,[35,36] can be approximated as $-u_{ij}^{\mathrm{S}}(r)$ derived in Sec. **2.2** (with the case of $r < |R_i - R_j|$ missed);[33] that this gives the different result of $c_{ij}(r) = -Z_i Z_j u^{\mathrm{C}}(r)$ for $r > R_i + R_j$ from the MSA closure above leads to fCSM and tCSM[17] mentioned at the

end of Sec. **2.2**. Blum and Rosenfeld also pointed out that Eqs. (4)~(6) are equivalent to minimizing f_b^{EC} with respect to $\tilde{\Gamma}_b$ (*i.e.*, $\partial f_b^{EC}/\partial \tilde{\Gamma}_b = 0$).[33]

4.2 Inhomogeneous Systems

For inhomogeneous electrolytes (such as those confined between two hard surfaces) in equilibrium with a bulk solution having densities $\{\rho_{i,b}\}$, Kierlik and Rosinberg,[5] as well as Rosenfeld,[37] proposed the bulk fluid density (BFD) method in early 1990s, where the system excess Helmholtz free energy due to the electrostatic correlations is approximated by a quadratic functional expansion around the bulk solution, *i.e.*, $F_{BFD}^{EC}[\{\rho_i\}] = f_b^{EC}\tilde{V} + \sum_i \mu_{i,b}^{EC}\int d\mathbf{r}\left(\rho_i(\mathbf{r}) - \rho_{i,b}\right) - (1/2)\sum_{i,j}\int d\mathbf{r}d\mathbf{r}'(\rho_i(\mathbf{r}) - \rho_{i,b})c_{ij}^{EC}(|\mathbf{r}-\mathbf{r}'|)\left(\rho_j(\mathbf{r}') - \rho_{j,b}\right)$, with f_b^{EC}, $\mu_{i,b}^{EC}$ and the direct PCF due to the electrostatic correlations $c_{ij}^{EC}(r) = c_{ij}(r) - c_{ij}^{PY}(r) + Z_iZ_ju^C(r)$ between CHSs of species *i* and *j* in the bulk solution given by the analytical results of the MSA theory shown in Sec. **4.1**.

In 2002, Gillespie and co-workers proposed the reference fluid density (RFD) method, where an ***inhomogeneous*** reference system having $\{\rho_{i,r}(\mathbf{r})\}$ that satisfy the local charge neutrality $\sum_i Z_i\rho_{i,r}(\mathbf{r}) = 0$ is used instead of the bulk solution, *i.e.*, $F_{RFD}^{EC}[\{\rho_i\}] = F_r^{EC}[\{\rho_{i,r}\}] + \sum_i\int d\mathbf{r}\mu_{i,r}^{EC}(\mathbf{r})\Delta\rho_i(\mathbf{r}) - (1/2)\sum_{i,j}\int d\mathbf{r}d\mathbf{r}'\Delta\rho_i(\mathbf{r})c_{ij,r}^{EC}(\mathbf{r},\mathbf{r}')\Delta\rho_j(\mathbf{r}')$, with F_r^{EC}, $\mu_{i,r}^{EC}(\mathbf{r}) \equiv \delta F_r^{EC}/\delta\rho_{i,r}(\mathbf{r})$, and $c_{ij,r}^{EC}(\mathbf{r},\mathbf{r}') \equiv -\delta^2F_r^{EC}/\delta\rho_{i,r}(\mathbf{r})\delta\rho_{j,r}(\mathbf{r}')$ being, respectively, the excess Helmholtz free energy, excess chemical potential of species *i*, and the direct PCF between species *i* and *j* due to the electrostatic correlations in the reference system, and $\Delta\rho_i(\mathbf{r}) \equiv \rho_i(\mathbf{r}) - \rho_{i,r}(\mathbf{r})$.[13,14] In particular, they took $\rho_{i,r}(\mathbf{r}) = \int d\mathbf{r}'\alpha_i(\mathbf{r}')\rho_i(\mathbf{r}')\Theta(R_c(\mathbf{r}) - |\mathbf{r}'-\mathbf{r}|)/(4\pi/3)R_c^3(\mathbf{r})$, where $\alpha_i(\mathbf{r}) = A(\mathbf{r})$ if $Z_i \geq 0$ and $\alpha_i(\mathbf{r}) = A(\mathbf{r})B(\mathbf{r})$ otherwise with $A(\mathbf{r}) = \sum_i Z_i^2\rho_i(\mathbf{r})/\left(\sum_{i\in\{Z_i>0\}} Z_i^2\rho_i(\mathbf{r}) + B(\mathbf{r})\sum_{i\in\{Z_i<0\}} Z_i^2\rho_i(\mathbf{r})\right)$ and $B(\mathbf{r}) = -\sum_{i\in\{Z_i>0\}} Z_i\rho_i(\mathbf{r})/\sum_{i\in\{Z_i<0\}} Z_i\rho_i(\mathbf{r})$ such that the fluid having densities $\{\alpha_i(\mathbf{r})\rho_i(\mathbf{r})\}$ is locally charge neutral (so is the reference fluid) and has the same ionic strength at each $\mathbf{r}$ as the system having $\{\rho_i(\mathbf{r})\}$, and $R_c(\mathbf{r}) = \sum_i \alpha_i(\mathbf{r})\rho_i(\mathbf{r})\tilde{\sigma}_i/2\sum_i \alpha_i(\mathbf{r})\rho_i(\mathbf{r}) + 1/2\tilde{\Gamma}(\mathbf{r})$; used the analytical results of the MSA theory shown in Sec. **4.1** but with $\rho_{i,b}$, $\tilde{\Gamma}_b$, $X_{i,b}$ and $\tilde{\eta}_b$ there replaced by $\rho_{i,r}(\mathbf{r})$, $\tilde{\Gamma}(\mathbf{r})$, $X_i(\mathbf{r})$ and $\tilde{\eta}(\mathbf{r})$, respectively, to obtain $\mu_{i,r}^{EC}(\mathbf{r})$ (note that since $\tilde{\Gamma}(\mathbf{r})$ depends on $\rho_{i,r}(\mathbf{r})$, it was solved iteratively from Eqs. (4)–(6) at each $\mathbf{r}$; and used the approximate result of Ref. [33] to obtain $c_{ij,r}^{EC}(\mathbf{r},\mathbf{r}')$, *i.e.*, $c_{ij,r}^{EC}(\mathbf{r},\mathbf{r}') \approx -\Delta u_{ij}(|\mathbf{r}-\mathbf{r}'|)$.[13,14]

In 2016, Roth and Gillespie proposed the functionalized MSA (fMSA) method by writing the system excess Helmholtz free energy due to the electrostatic correlations as $F_{fMSA}^{EC}[\{\rho_i\}] = \int d\mathbf{r}\Phi_{fMSA}^{EC}(\{m_{2,i}(\mathbf{r})\})$ with $\Phi_{fMSA}^{EC}(\mathbf{r})$, which is a ***function*** of the weighted densities $m_{2,i}(\mathbf{r}) \equiv (\tilde{\sigma}_i/2R_i)^2\int d\mathbf{r}'\rho_i(\mathbf{r}')\tilde{w}_2(|\mathbf{r}-\mathbf{r}'|;R_i)$ with $R_i \equiv \tilde{\sigma}_i/2 + 1/2\tilde{\Gamma}_b$ and $\tilde{\Gamma}_b$ solved directly from Eqs. (4)~(6), obtained from f_b^{EC} of the MSA theory by replacing $\rho_{i,b}$ there with $m_{2,i}(\mathbf{r})/\pi\tilde{\sigma}_i^2$; that is,

$$\Phi_{fMSA}^{EC}(\mathbf{r}) = \frac{\tilde{\Gamma}^3(\mathbf{r})}{3\pi} - \frac{1}{\pi\tilde{\varepsilon}}\sum_i \frac{m_{2,i}(\mathbf{r})Z_i\left(Z_i - X_i(\mathbf{r})\right)}{\tilde{\sigma}_i^3} \tag{8}$$

where $\tilde{\Gamma}(\mathbf{r})$ is solved at each $\mathbf{r}$ from Eqs. (4)~(6) with $\rho_{i,b}$, $\tilde{\Gamma}_b$, $X_{i,b}$ and $\tilde{\eta}_b$ there replaced by $m_{2,i}(\mathbf{r})/\pi\tilde{\sigma}_i^2$, $\tilde{\Gamma}(\mathbf{r})$, $X_i(\mathbf{r})$ and $\tilde{\eta}(\mathbf{r})$, respectively.[15,16] They also used F_{CSM}^{MF} (where the case of $r < |R_i - R_j|$ was missed in their CSM as mentioned in Sec. **2.2**) instead of F_{PCM}^{MF} in their F^{ex}; by comparing with MC simulations of monovalent and symmetric electrolytes near a charged hard surface[38], they showed that using F_{tCSM}^{MF} (*i.e.*, $F^{ex} = F_{tCSM}^{MF} + F_{mFMT}^{HS} + F_{fMSA}^{EC}$) gives better results than using F_{fCSM}^{MF}.[15]

Gillespie and co-workers quantitatively compared DFT predictions using the above BFD, RFD and fMSA methods with extensive MC simulations of electrolytes (having monovalent anions) near a hard surface[39], and found that overall RFD is the best, BFD is the least accurate, and fMSA is significantly better than BFD, making it a reasonable choice that is less computationally expensive than RFD.[40] For monovalent cations, all three DFTs work reasonably well, except that the BFD predictions are qualitatively different from MC results at very low surface charge densities. For multivalent cations, BFD tends to significantly underestimate the charge inversion while fMSA overestimates it. All three DFTs perform poorly for small trivalent cations.[40]

In 2018, Jiang *et al.*[41,42] (JGW) used the 1st-order Taylor expansion $\Phi_{JGW}^{EC}(\{\rho_i(\mathbf{r})\}) = \Phi_r^{EC}(\{\rho_{i,r}(\mathbf{r})\}) + \sum_i \frac{\partial\Phi_r^{EC}(\{\rho_{i,r}(\mathbf{r})\})}{\partial\rho_{i,r}(\mathbf{r})}\Delta\rho_i(\mathbf{r})$ (thus $F_{JGW}^{EC}[\{\rho_i\}] = \int d\mathbf{r}\Phi_{JGW}^{EC}(\mathbf{r})$) around the inhomogeneous reference fluid having $\{\rho_{i,r}(\mathbf{r})\}$ given by the RFD method,[13,14] where $\Phi_r^{EC}(\{\rho_{i,r}(\mathbf{r})\}) = \tilde{\Gamma}^3(\mathbf{r})/3\pi - (1/\tilde{\varepsilon})\sum_i \rho_{i,r}(\mathbf{r})Z_i\left(Z_i - X_i(\mathbf{r})\right)/\tilde{\sigma}_i$ (which can be compared with Eq. (8)) with the same expressions for $\tilde{\Gamma}(\mathbf{r})$, $X_i(\mathbf{r})$ and $\tilde{\eta}(\mathbf{r})$ as given by the RFD method,[13,14] and $\partial\Phi_r^{EC}(\{\rho_{i,r}(\mathbf{r})\})/\partial\rho_{i,r}(\mathbf{r})$ is given in the **Appendix**. They showed by comparing with MC simulations of symmetric electrolytes near a charged hard surface and asymmetric electrolytes near a uncharged hard surface[43] that their method gives comparable results to RFD with only moderate quantitative differences when the contribution from the electrostatic correlations is important (*i.e.*, for highly charged surfaces, large Bjerrum length, high valence, and intermediate ion concentrations), but is easier to implement than RFD.[41]

In 2021, Jiang and Gillespie[17] corrected the missing case in CSM and proposed a modified version of fMSA (referred to as mfMSA), where they obtained the local excess Helmholtz free-energy density due to the electrostatic correlations $\Phi_{mfMSA}^{EC}(\mathbf{r})$ from f_b^{EC} of the MSA theory by replacing $\rho_{i,b}$ and $\xi_{3,i} \equiv \pi\rho_{i,b}\tilde{\sigma}_i^3/6$ there with $m_{2,i}(\mathbf{r})/\pi\tilde{\sigma}_i^2$ and another weighted density $m_{3,i}(\mathbf{r}) \equiv (\tilde{\sigma}_i/2R_i)^3\int d\mathbf{r}'\rho_i(\mathbf{r}')w_3(|\mathbf{r}-\mathbf{r}'|;R_i)$, respectively (note that four ***dimensional*** weighted densities $(\sigma_i/2R_i)^\alpha\int d\mathbf{r}'\rho_i(\mathbf{r}')w_\alpha(|\mathbf{r}-\mathbf{r}'|;R_i)$ for α=0, 1, 2, 3 are used in Ref. [17], which are similar to $n_{\alpha,i}(\mathbf{r})$ mentioned in Sec. **3**); this gives the same expression of $\Phi_{mfMSA}^{EC}(\mathbf{r})$ as Eq. (8) (thus $F_{mfMSA}^{EC}[\{\rho_i\}] = \int d\mathbf{r}\Phi_{mfMSA}^{EC}(\{m_{2,i}(\mathbf{r}), m_{3,i}(\mathbf{r})\})$), but with $\tilde{\eta}(\mathbf{r}) = \sum_i \frac{Z_im_{2,i}(\mathbf{r})}{\tilde{\sigma}_i\left(1 + \tilde{\Gamma}(\mathbf{r})\tilde{\sigma}_i\right)}\Big/\left[2 + 2\sum_i \frac{m_{3,i}(\mathbf{r})\left(2 - \tilde{\Gamma}(\mathbf{r})\tilde{\sigma}_i\right)}{1 + \tilde{\Gamma}(\mathbf{r})\tilde{\sigma}_i}\right]$ different from that given by the fMSA method.[17] By comparing the

density profiles of cations near a charged hard surface, they found that fMSA and mfMSA give basically the same result. They also compared their mfMSA predictions using PCM, fCSM and tCSM, as well as the BFD predictions, with extensive MC simulations of electrolytes near a hard surface,[39] and found that their DFT with $F^{ex} = F^{MF}_{tCSM} + F^{HS}_{mFMT} + F^{EC}_{mfMSA}$ gives overall the best agreement with MC results while the PCM and BFD predictions are generally far worse;[17] that using tCSM gives better predictions than using fCSM or PCM can be attributed to the inaccuracy of F^{EC}_{mfMSA} in describing the electrostatic correlations in the system.

5 CORRELATIONS FOR PEs (CHARGED THSCs) DUE TO CHAIN CONNECTIVITY

For CHSs, $y_{ii}(\tilde{\sigma}_i) = g_{ii}(\tilde{\sigma}_i)\exp\left(Z_i^2/\tilde{\varepsilon}\tilde{\sigma}_i\right)$; since $g^{MSA}_{ii}(\tilde{\sigma}_i)$ is not very accurate and can even be negative for small $\tilde{\varepsilon}$ or low ionic densities, the exponential (EXP) approximation[44] $g^{EXP}_{ii}(\tilde{\sigma}_i) = g^{PY}_{ii}(\tilde{\sigma}_i)\exp\left(g^{MSA}_{ii}(\tilde{\sigma}_i) - g^{PY}_{ii}(\tilde{\sigma}_i)\right)$ can be used instead, which gives $y_{ii}(\tilde{\sigma}_i) = g^{PY}_{ii}(\tilde{\sigma}_i)\exp\left[\left(Z_i^2 - X_{i,b}{}^2\right)/\tilde{\varepsilon}\tilde{\sigma}_i\right]$ according to Eq. (7). TPT1 with the EXP approximation therefore gives $f^{CH} = f^{CH,HS} + f^{CH,EC}$ with $f^{CH,HS} = \sum_i (1/N_i - 1)\rho_{i,b}\ln g^{PY}_{ii}(\tilde{\sigma}_i)$ and $f^{CH,EC} = (1/\tilde{\varepsilon})\sum_i (1/N_i - 1)\rho_{i,b}\left(Z_i^2 - X_{i,b}{}^2\right)/\tilde{\sigma}_i$.

In 2006, Li and Wu[45,46] (LW) proposed a PDFT for inhomogeneous PE systems; they used F^{MF}_{PCM}, F^{HS}_{mFMT} and F^{EC}_{BFD} (thus neglecting the effects of chain connectivity on $c^{EC}_{ij}(r)$), and extended TPT1 to inhomogeneous systems by writing their excess Helmholtz free energy due to the chain connectivity $F^{CH}_{LW}[\{\rho_i\}] = \int d\mathbf{r}\Phi^{CH}_{LW}(\mathbf{r})$, where $\Phi^{CH}_{LW}(\mathbf{r})$ is obtained from f^{CH} of TPT1 under the EXP approximation[44] with $\rho_{i,b}$, $\rho_{i,b}\tilde{\sigma}_i$, $\tilde{\xi}_2$ and $\xi_{3,i}$ there replaced by $\zeta_i(\mathbf{r})\tilde{n}_{2,i}(\mathbf{r})/\pi\tilde{\sigma}_i^2$, $\tilde{n}_{2,i}(\mathbf{r})/\pi\tilde{\sigma}_i$, $\zeta(\mathbf{r})\tilde{n}_2(\mathbf{r})$ and $n_{3,i}(\mathbf{r})$ (thus $\tilde{\Gamma}_b$, $\tilde{\eta}_b$, $X_{i,b}$ and $y_{ii}(\tilde{\sigma}_i)$ by $\tilde{\Gamma}(\mathbf{r})$, $\tilde{\eta}(\mathbf{r})$, $X_i(\mathbf{r})$ and $y_{ii}(\mathbf{r};\tilde{\sigma}_i)$), respectively; this gives $\Phi^{CH}_{LW}(\mathbf{r}) = \sum_i \frac{\zeta_i(\mathbf{r})\tilde{n}_{2,i}(\mathbf{r})}{\pi\tilde{\sigma}_i^2}\left(\frac{1}{N_i} - 1\right)\left[\ln\left(\frac{1}{1-n_3(\mathbf{r})} + \frac{\tilde{\sigma}_i\zeta(\mathbf{r})\tilde{n}_2(\mathbf{r})}{4(1-n_3(\mathbf{r}))^2}\right) + \frac{Z_i^2 - X_i^2(\mathbf{r})}{\tilde{\varepsilon}\tilde{\sigma}_i}\right]$, $\tilde{\Gamma}(\mathbf{r}) = \sqrt{(1/\tilde{\varepsilon})\sum_i \tilde{n}_{2,i}(\mathbf{r})X_i{}^2(\mathbf{r})/\tilde{\sigma}_i^2}$, the same expression for $X_i(\mathbf{r})$ as in Sec. **4.2**, and $\tilde{\eta}(\mathbf{r}) = \sum_i \frac{Z_i\tilde{n}_{2,i}(\mathbf{r})}{\tilde{\sigma}_i\left(1 + \tilde{\Gamma}(\mathbf{r})\tilde{\sigma}_i\right)}\Big/\left[2 + 2\sum_i \frac{n_{3,i}(\mathbf{r})\left(2 - \tilde{\Gamma}(\mathbf{r})\tilde{\sigma}_i\right)}{1 + \tilde{\Gamma}(\mathbf{r})\tilde{\sigma}_i}\right]$. They compared their PDFT predictions with MC simulations[47] of monovalent systems (*i.e.*, $|Z_i|$=1) of PEs each having N=10 segments near an oppositely charged hard surface without salt (where $\tilde{\sigma}_i = \tilde{\varepsilon} = 1$) and found good agreement in the density profiles of PE segments and ions at various surface charge densities and PE concentrations in the bulk solution.[45,46] Jiang and Wu also reported similar comparisons for trivalent counterions (where $\tilde{\sigma}_i = 1$ and $\tilde{\varepsilon} \approx 0.595$) at two PE concentrations in the bulk solution.[48]

In 2018, Jiang *et al.*[41,42] showed that the above method of extending TPT1 to inhomogeneous PE systems is only appropriate when the electrostatic interactions are weak or when the non-bonded interactions are dominated by the HS contribution, and proposed their excess Helmholtz free energy due to the chain connectivity as $F^{CH}_{JGW}[\{\rho_i\}] = \int d\mathbf{r}(\Phi^{CH,HS}(\mathbf{r}) + \Phi^{CH,EC}_{JGW}(\mathbf{r}))$, where $\Phi^{CH,HS}(\mathbf{r})$ is obtained from f^{CH} of TPT1 for bulk mixtures of ***uncharged*** THSCs given in Sec. **3** with $\rho_{i,b}$ and ξ_3 there replaced by $\tilde{n}_{2,i}(\mathbf{r})/\pi\tilde{\sigma}_i^2$ and $n_3(\mathbf{r})$, respectively, *i.e.*, $\Phi^{CH,HS}(\mathbf{r}) = \sum_i \frac{\tilde{n}_{2,i}(\mathbf{r})}{\pi\tilde{\sigma}_i^2}\left(\frac{1}{N_i} - 1\right)\ln\left[\frac{1}{1-n_3(\mathbf{r})} + \frac{\tilde{\sigma}_i\tilde{n}_2(\mathbf{r})}{4(1-n_3(\mathbf{r}))^2} + \frac{\tilde{\sigma}_i^2\tilde{n}_2^2(\mathbf{r})}{72(1-n_3(\mathbf{r}))^3}\right]$ (which can be compared with Eq. (3)), and $\Phi^{CH,EC}_{JGW}(\{\rho_i(\mathbf{r})\}) = \Phi^{CH,EC}_r(\{\rho_{i,r}(\mathbf{r})\}) + \sum_i \frac{\partial\Phi^{CH,EC}_r(\{\rho_{i,r}(\mathbf{r})\})}{\partial\rho_{i,r}(\mathbf{r})}\Delta\rho_i(\mathbf{r})$ with $\Phi^{CH,EC}_r(\{\rho_{i,r}(\mathbf{r})\}) = (1/\tilde{\varepsilon})\sum_i \rho_{i,r}(\mathbf{r})(1/N_i - 1)\left(Z_i^2 - X_i^2(\mathbf{r})\right)/\tilde{\sigma}_i$ and $\partial\Phi^{CH,EC}_r(\{\rho_{i,r}(\mathbf{r})\})/\partial\rho_{i,r}(\mathbf{r})$ given in the **Appendix** (which is consistent with their $\Phi^{EC}_{JGW}(\{\rho_i(\mathbf{r})\})$ given in Sec. **4.2**).

More recently, Chang and Jiang wrote their excess Helmholtz free energy due to the chain connectivity as $F^{CH}_{CJ}[\{\rho_i\}] = \int d\mathbf{r}(\Phi^{CH,HS}(\mathbf{r}) + \Phi^{CH,EC}_{mfMSA}(\{m_{2,i}(\mathbf{r}), m_{3,i}(\mathbf{r})\}))$, where $\Phi^{CH,EC}_{mfMSA}(\mathbf{r})$ is obtained from $f^{CH,EC}$ of TPT1 with $\rho_{i,b}$ and $\xi_{3,i}$ there replaced by $m_{2,i}(\mathbf{r})/\pi\tilde{\sigma}_i^2$ and $m_{3,i}(\mathbf{r})$, respectively, in the same way as the mfMSA method.[49] For block polyelectrolytes (BPEs) that they studied, where each chain of species i consists of N_B blocks with block k (=1, …, N_B) having N_k segments of valence Z_k (note that N_B, k, N_k and Z_k all depend on i), Eq. (2) becomes $f^{CH} = \sum_i\left(\rho_{i,b}/N_i\right)\left[\sum_{k=1}^{N_B}(1-N_k)\ln y_{k,k}(\tilde{\sigma}_i) - \sum_{k=1}^{N_B-1}\ln y_{k,k+1}(\tilde{\sigma}_i)\right]$ with $y_{k,k'}(\tilde{\sigma}_i) = g_{ii}(\tilde{\sigma}_i)\exp\left(Z_kZ_{k'}/\tilde{\varepsilon}\tilde{\sigma}_i\right)$ being the contact value of the CCF between segments in block k and those in block k' of species i; they therefore obtained $\Phi^{CH,EC}_{mfMSA}(\mathbf{r}) = (1/\pi\tilde{\varepsilon})\sum_i\left(m_{2,i}(\mathbf{r})/N_i\tilde{\sigma}_i^3\right)\left[\sum_{k=1}^{N_B}(1-N_k)\left(Z_k^2 - X_k^2(\mathbf{r})\right) - \sum_{k=1}^{N_B-1}\left(Z_kZ_{k+1} - X_k(\mathbf{r})X_{k+1}(\mathbf{r})\right)\right]$.[49] Qing and Jiang, however, wrote their excess Helmholtz free energy due to the chain connectivity as $F^{CH}_{QJ}[\{\rho_i\}] = \int d\mathbf{r}(\Phi^{CH}(\mathbf{r}) + \Phi^{CH,EC}_{MSA}(\{m_{2,i}(\mathbf{r})\}))$, where $\Phi^{CH}(\mathbf{r})$ is given by Eq. (3) and $\Phi^{CH,EC}_{MSA}(\{m_{2,i}(\mathbf{r})\})$ is obtained from $f^{CH,EC}$ of TPT1 with $\rho_{i,b}$ replaced by $m_{2,i}(\mathbf{r})/\pi\tilde{\sigma}_i^2$ but $X_{i,b}$ unchanged; this gives $\Phi^{CH,EC}_{MSA}(\mathbf{r}) = (1/\pi\tilde{\varepsilon})\sum_i\left(m_{2,i}(\mathbf{r})/N_i\tilde{\sigma}_i^3\right)\left[\sum_{k=1}^{N_B}(1-N_k)\left(Z_k{}^2 - X_{k,b}{}^2\right) - \sum_{k=1}^{N_B-1}\left(Z_kZ_{k+1} - X_{k,b}X_{k+1,b}\right)\right]$ for the BPEs.[50]

6 APPLICATIONS OF VARIOUS PDFTs OF PE SYSTEMS

Unless specified otherwise, in all PDFTs of PEs, the PEs are modelled as charged THSCs, the ions as CHSs, and the confining surfaces as hard and flat surfaces; all PDFT calculations of PE systems have been performed in 1D.

Li and Wu proposed their PDFT with $F^{ex} = F^{MF}_{PCM} + F^{HS}_{mFMT} + F^{EC}_{BFD} + F^{CH}_{LW}$ and applied it to salt-free PE systems near an oppositely charged hard surface.[45–46] Wu and co-workers then applied it to study the effects of chain length and grafting density, counterion valence and size, and bulk salt concentration on PE brushes grafted onto a uncharged surface,[48,51,52] as well as the effects of chain length, counterion valence, surface charge density, and bulk salt concentration on the PE ad-

sorption at both oppositely and likely charged surfaces.[53]

Wu and co-workers also applied their PDFT to study the osmotic pressure and radial distribution of double-stranded DNA confined in λ-bacteriophages (modelled as an uncharged spherical shell, with an extra term in F^{ex} accounting for the van der Waals attraction between PE segments and ions *via* the mean-field approximation)[54], the electrostatic regulation of pregenomic RNA packaging in Hepatitis B virus nucleocapsid (modelled as a charged spherical shell with grafted and charged THSCs representing the highly flexible C-terminal domain chains),[55] and the radial distributions of the C-terminal domain chains and nucleic acids (modelled as charged THSCs with a bending potential) in the Hepatitis B virus nucleocapsid at the beginning and final stages of viral reverse transcription.[56] More recently, Cheng *et al*. applied this PDFT[45,46] to study the competitive adsorption between surfactants (modeled as THSCs each of ten segments with only one end-segment negatively charged) and polyanion (sodium polyacrylate) chains on an oppositely charged (rock) surface and in rock crevices, and found the optimal chain length and concentration for reducing the surfactant adsorption in the process of chemical-enhanced oil recovery.[57]

Jiang *et al*. proposed their PDFT with $F^{ex} = F^{MF}_{PCM} + F^{HS}_{mFMT} + F^{EC}_{JGW} + F^{CH}_{JGW}$ and applied it to salt-free PE systems confined between two uncharged surfaces.[41] They also applied a variant of their PDFT to incompressible PE solutions, where solvent molecules are explicitly included as uncharged HSs under the constraint of $\sum_i \tilde{\sigma}_i^3 \rho_i(\mathbf{r})$ being a constant at all **r**, confined between either uncharged surfaces to study the origin of oscillatory mediated interactions between the surfaces[42] or likely charged surfaces (having the same type of charges as the PEs) with a modified 9-3 potential attractive for the PEs to study their non-electrostatic adsorption and mediated interactions between the surfaces[58]; in this case F^{HS}_{mFMT} is omitted, and their $\rho_{i,r}(\mathbf{r})$ for the solvent is chosen such that the reference fluid is also incompressible.

Chang and Jiang proposed their PDFT with $F^{ex} = F^{MF}_{tCSM} + F^{HS}_{mFMT} + F^{EC}_{mfMSA} + F^{CH}_{CJ}$ and applied it to study the effects of block length and sequence on the salt-enhanced adsorption of BPEs consisting of (positively) charged and uncharged blocks at an oppositely charged surface.[49] They subsequently applied it to analyze the microstructures of such BPEs confined between two identical and (negatively) charged surfaces, and the relationship between the block length and sequence and the BPE-mediated attractive forces between the surfaces.[59] Most recently, they applied a variant of their PDFT with $F^{ex} = F^{MF}_{tCSM} + F^{HS}_{mFMT} + F^{EC}_{BFD} + F^{CH}_{CJ}$ to study systems similar to those in Ref. [59] but with short negatively charged PEs added to enhance the adhesive strength at high salt concentrations.[60]

Qing and Jiang applied a PDFT with $F^{ex} = F^{MF}_{PCM} + F^{HS}_{mFMT} + F^{CH}$, where F^{CH} is given in Sec. **3** but extended to uncharged block copolymers (that is, the electrostatic correlations are neglected here), to BPE brushes consisting of charged and uncharged blocks grafted onto a uncharged surface.[61] In a subsequent work they included the electrostatic correlations, *i.e.*, $F^{ex} = F^{MF}_{PCM} + F^{HS}_{mFMT} + F^{EC}_{mfMSA} + F^{CH}_{QJ}$, and studied the effects of chain length and grafting density, brush composition, bulk salt concentration and surface voltage on the structure and energy-storage capacity of BPE brushes and mixed brushes consisting of uncharged and PE (either polyanion or polycation) chains.[50]

Most recently, Wu and co-workers applied a variant of their PDFT with $F^{ex} = F^{MF}_{PCM} + F^{HS}_{mFMT} + F^{EC}_{RFD} + F^{CH}_{LW}$ to study the effects of chain length and grafting density, counterion size and valence, and salt concentration on the surfaces forces and swelling behavior of two identical and opposing PE brushes each grafted onto a uncharged surface.[62]

7 SOME PERSPECTIVES ON FUTURE WORK

It is clear from the above that PDFTs have distinct advantages in the study of PE systems over experiments and molecular simulations. In great contrast to the well-developed and now routinely performed 3D SCFT calculations, however, PDFT calculations have been much less developed and applied in the literature; 2D[63,64] and 3D[65] PDFT calculations have rarely been performed, mainly due to the inefficient numerical methods used. In fact, for long chains SCFT and PDFT calculations have comparable computational cost, most of which are for solving the propagators. Implementing some of the efficient numerical methods[66–68] recently developed for SCFT calculations can therefore readily enable 3D PDFT calculations.

Also in great contrast to the systematic and comprehensive assessment,[17,40] *via* quantitative comparisons with MC simulations of the same model system as used in DFTs, of the various functional forms proposed for treating the electrostatic correlations in electrolytes, such assessment on treating the chain correlations in PE systems is lacking, particularly for chains longer than 10 segments. This is in part due to the scarce MC simulation data of charged THSCs[69–74] reported in the literature, as most molecular simulations of PE systems use different models than that of charged THSCs to avoid the restriction of fixed bond length and the discontinuity of HS potential (thus to take advantage of the efficient parallelization provided by general molecular dynamics simulation packages). Quantitatively assessing the existing PDFTs against such simulation results therefore calls for a carefully designed procedure that minimizes the ambiguity of parameter-fitting between the different models. On the other hand, it is desirable to develop other versions of PDFTs that are not based on the THSC model, such as that proposed by Chandler and co-workers[75,76] and its variant.[6,8,77]

Last but not least, given that the shortcomings of TPT1 are well-known,[23] it is also desirable to develop more accurate approaches for treating the chain correlations, which would be useful for longer chains. Another way to better capture the chain conformations is the self-consistent PDFT calculation,[78,79] which combines single-chain simulations with PDFT calculations but has not been applied to PE systems yet; note that, while molecular simulations are computationally much more intensive than PDFT calculations, such single-chain simulations are still orders of magnitude faster than the many-chain simulations, especially for long-chain PE systems.

https://doi.org/10.1007/s10118-024-3197-2

Appendix:

Here we follow our notation in the main text and derive $\frac{\partial\Phi_r^{EC}(\mathbf{r})}{\partial\rho_{i,r}(\mathbf{r})}$ in $\Phi_{JGW}^{EC}(\{\rho_i(\mathbf{r})\})$ and $\frac{\partial\Phi_r^{CH,EC}(\mathbf{r})}{\partial\rho_{i,r}(\mathbf{r})}$ in $\Phi_{JGW}^{CH,EC}(\{\rho_i(\mathbf{r})\})$ proposed in Ref. [41]. From $\Phi_r^{EC}(\{\rho_{i,r}(\mathbf{r})\}) = \tilde{\Gamma}^3(\mathbf{r})/3\pi - (1/\tilde{\varepsilon})\sum_j \rho_{j,r}(\mathbf{r})Z_j\left(Z_j - X_j(\mathbf{r})\right)/\tilde{\sigma}_j$ and $\Phi_r^{CH,EC}(\{\rho_{i,r}(\mathbf{r})\}) = (1/\tilde{\varepsilon})\sum_j \rho_{j,r}(\mathbf{r})\left(1/N_j - 1\right)\left(Z_j^2 - X_j^2(\mathbf{r})\right)/\tilde{\sigma}_j$, we find

$$\frac{\partial\Phi_r^{EC}(\mathbf{r})}{\partial\rho_{i,r}(\mathbf{r})} = \frac{\tilde{\Gamma}^2(\mathbf{r})}{\pi}\frac{\partial\tilde{\Gamma}(\mathbf{r})}{\partial\rho_{i,r}(\mathbf{r})} - \frac{1}{\tilde{\varepsilon}}\left[\frac{Z_i\left(Z_i - X_i(\mathbf{r})\right)}{\tilde{\sigma}_i} - \sum_j \rho_{j,r}(\mathbf{r})Z_j\frac{\partial X_j(\mathbf{r})/\tilde{\sigma}_j}{\partial\rho_{i,r}(\mathbf{r})}\right] \tag{9}$$

and $\frac{\partial\Phi_r^{CH,EC}(\mathbf{r})}{\partial\rho_{i,r}(\mathbf{r})} = \frac{1}{\tilde{\varepsilon}}\left[\left(\frac{1}{N_i} - 1\right)\frac{Z_i^2 - X_i^2(\mathbf{r})}{\tilde{\sigma}_i} - 2\sum_j \rho_{j,r}(\mathbf{r})\left(\frac{1}{N_j} - 1\right)X_j(\mathbf{r})\frac{\partial X_j(\mathbf{r})/\tilde{\sigma}_j}{\partial\rho_{i,r}(\mathbf{r})}\right]$, respectively.

To obtain $\frac{\partial X_j(\mathbf{r})/\tilde{\sigma}_j}{\partial\rho_{i,r}(\mathbf{r})}$, we first introduce $a_j(\mathbf{r}) \equiv (1/\tilde{\sigma}_j + \tilde{\Gamma}(\mathbf{r}))^{-1}$ for each species j, which gives $\frac{\partial a_j(\mathbf{r})}{\partial\rho_{i,r}(\mathbf{r})} = -a_j^2(\mathbf{r})\frac{\partial\tilde{\Gamma}(\mathbf{r})}{\partial\rho_{i,r}(\mathbf{r})}$, then from $X_j(\mathbf{r}) = \tilde{\sigma}_j a_j(\mathbf{r})(Z_j/\tilde{\sigma}_j^2 - \tilde{\eta}(\mathbf{r}))$ (which can be compared to Eq. (5)) we find $\frac{\partial X_j(\mathbf{r})/\tilde{\sigma}_j}{\partial\rho_{i,r}(\mathbf{r})} = -a_j(\mathbf{r})\left(\frac{\partial\tilde{\eta}(\mathbf{r})}{\partial\rho_{i,r}(\mathbf{r})} + \frac{X_j(\mathbf{r})}{\tilde{\sigma}_j}\frac{\partial\tilde{\Gamma}(\mathbf{r})}{\partial\rho_{i,r}(\mathbf{r})}\right)$. Similarly, to obtain $\frac{\partial\tilde{\eta}(\mathbf{r})}{\partial\rho_{i,r}(\mathbf{r})}$, we first introduce $a(\mathbf{r}) \equiv 2/\pi + \sum_j \tilde{\sigma}_j^2\rho_{j,r}(\mathbf{r})a_j(\mathbf{r})(2 - \tilde{\sigma}_j\tilde{\Gamma}(\mathbf{r}))/3$, which with the above results gives $\frac{\partial a(\mathbf{r})}{\partial\rho_{i,r}(\mathbf{r})} = \frac{1}{3}\tilde{\sigma}_i^2 a_i(\mathbf{r})(2 - \tilde{\sigma}_i\tilde{\Gamma}(\mathbf{r})) - \sum_j \tilde{\sigma}_j^2\rho_{j,r}(\mathbf{r})a_j^2(\mathbf{r})\frac{\partial\tilde{\Gamma}(\mathbf{r})}{\partial\rho_{i,r}(\mathbf{r})}$, then from $\tilde{\eta}(\mathbf{r}) = \sum_j Z_j\rho_{j,r}(\mathbf{r})a_j(\mathbf{r})/a(\mathbf{r})$ (which can be compared to Eq. (6)) we obtain after some manipulation $\frac{\partial\tilde{\eta}(\mathbf{r})}{\partial\rho_{i,r}(\mathbf{r})} = \frac{1}{a(\mathbf{r})}\left\{a_i(\mathbf{r})\left[Z_i - \frac{\tilde{\sigma}_i^2}{3}\tilde{\eta}(\mathbf{r})\left(2 - \tilde{\sigma}_i\tilde{\Gamma}(\mathbf{r})\right)\right] - \sum_j \tilde{\sigma}_j\rho_{j,r}(\mathbf{r})a_j(\mathbf{r})X_j(\mathbf{r})\frac{\partial\tilde{\Gamma}(\mathbf{r})}{\partial\rho_{i,r}(\mathbf{r})}\right\}$. Finally, from

$$\tilde{\Gamma}^2(\mathbf{r}) = \frac{\pi}{\tilde{\varepsilon}}\sum_j \rho_{j,r}(\mathbf{r})X_j^2(\mathbf{r}) \tag{10}$$

which can be compared to Eq. (4), we obtain $\frac{\partial\tilde{\Gamma}(\mathbf{r})}{\partial\rho_{i,r}(\mathbf{r})} = \frac{\pi}{2\tilde{\varepsilon}\tilde{\Gamma}(\mathbf{r})}\left(X_i^2(\mathbf{r}) + 2\sum_j \tilde{\sigma}_j\rho_{j,r}(\mathbf{r})X_j(\mathbf{r})\frac{\partial X_j(\mathbf{r})/\tilde{\sigma}_j}{\partial\rho_{i,r}(\mathbf{r})}\right)$; with the above results of $\frac{\partial X_j(\mathbf{r})/\tilde{\sigma}_j}{\partial\rho_{i,r}(\mathbf{r})}$ and $\frac{\partial\tilde{\eta}(\mathbf{r})}{\partial\rho_{i,r}(\mathbf{r})}$, we can then obtain $\frac{\partial\tilde{\Gamma}(\mathbf{r})}{\partial\rho_{i,r}(\mathbf{r})} = \frac{X_i^2(\mathbf{r})/2 - a_i(\mathbf{r})\left[Z_i - \left(\tilde{\sigma}_i^2/3\right)\tilde{\eta}(\mathbf{r})\left(2 - \tilde{\sigma}_i\tilde{\Gamma}(\mathbf{r})\right)\right]b(\mathbf{r})/a(\mathbf{r})}{\tilde{\varepsilon}\tilde{\Gamma}(\mathbf{r})/\pi + \sum_j \rho_{j,r}(\mathbf{r})a_j(\mathbf{r})X_j^2(\mathbf{r}) - b^2(\mathbf{r})/a(\mathbf{r})}$, where $b(\mathbf{r}) \equiv \sum_j \tilde{\sigma}_j\rho_{j,r}(\mathbf{r})a_j(\mathbf{r})X_j(\mathbf{r})$, thus $\frac{\partial\Phi_r^{EC}(\mathbf{r})}{\partial\rho_{i,r}(\mathbf{r})}$ and $\frac{\partial\Phi_r^{CH,EC}(\mathbf{r})}{\partial\rho_{i,r}(\mathbf{r})}$.

Note, however, that $\frac{\partial\Phi_r^{EC}(\mathbf{r})}{\partial\rho_{i,r}(\mathbf{r})}$ is independent of $\frac{\partial\tilde{\Gamma}(\mathbf{r})}{\partial\rho_{i,r}(\mathbf{r})}$. Substituting the above results of $\frac{\partial X_j(\mathbf{r})/\tilde{\sigma}_j}{\partial\rho_{i,r}(\mathbf{r})}$ and $\frac{\partial\tilde{\eta}(\mathbf{r})}{\partial\rho_{i,r}(\mathbf{r})}$ into Eq. (9), we obtain after some manipulation $\frac{\partial\Phi_r^{EC}(\mathbf{r})}{\partial\rho_{i,r}(\mathbf{r})} = \left(\frac{\tilde{\Gamma}^2(\mathbf{r})}{\pi} - \frac{1}{\tilde{\varepsilon}}\sum_j \rho_{j,r}(\mathbf{r})X_j^2(\mathbf{r})\right)\frac{\partial\tilde{\Gamma}(\mathbf{r})}{\partial\rho_{i,r}(\mathbf{r})} - \frac{1}{\tilde{\varepsilon}}\left\{Z_i\frac{Z_i - X_i(\mathbf{r})}{\tilde{\sigma}_i} + \tilde{\eta}(\mathbf{r})a_i(\mathbf{r})\left[Z_i - \frac{\tilde{\sigma}_i^2}{3}\tilde{\eta}(\mathbf{r})\left(2 - \tilde{\sigma}_i\tilde{\Gamma}(\mathbf{r})\right)\right]\right\}$, where the first term on the right-hand-side vanishes according to Eq. (10); this is the same as $\mu_{i,r}^{EC}(\mathbf{r})$ in the RFD method or $\mu_{i,b}^{EC}$ in the BFD method (*i.e.*, with $\rho_{i,r}(\mathbf{r})=\rho_{i,b}$ for all i).

BIOGRAPHIES

Bao-Hui Li received her Ph.D. degree in the field of Condensed Matter Physics from Nankai University in 1994. Since then, she has been a faculty member in the School of Physics at Nankai University, and she was appointed as an Associate Professor and Professor in 1996 and 2001, respectively. She leads a Soft Matter group working on self-assembly, phases and phase transitions, and chain conformations and conformation transitions of macromolecules using molecular modeling and mean-field theory.

Qiang Wang received his Ph.D. degree in Chemical Engineering from University of Wisconsin–Madison in 2002 under the direction of Prof. Juan de Pablo and Prof. Paul Nealey. He then did postdoctoral research at University of California–Santa Barbara with Prof. Glenn Fredrickson. He has been appointed as an Assistant/Associate/Full Professor in the Department of Chemical and Biological Engineering at Colorado State University since 2004. He leads the Laboratory of Computational Soft Materials there studying the behavior of nanostructured polymeric materials.

Conflict of Interests

The authors declare no interest conflict.

ACKNOWLEDGMENTS

We thank Prof. Jian Jiang for his careful reading of this manuscript. BHL acknowledges the financial support for this work provided by the National Natural Science Foundation of China (Nos. 22173051 and 21829301). QW also acknowledges the donors of The American Chemical Society Petroleum Research Fund for partial support of this work.

REFERENCES

1 Fredrickson, G. H. *The equilibrium theory of inhomogeneous polymers*. Oxford University Press: New York, **2006**.
2 Hohenberg, P.; Kohn, W. Inhomogeneous electron gas. *Phys. Rev.* **1964**, *136*, B864–B871.
3 Mermin, N. D. Thermal properties of the inhomogeneous electron gas. *Phys. Rev.* **1965**, *137*, A1441–A1443.
4 Woodward, C. E. A density functional theory for polymers: application to hard chain-hard sphere mixtures in slitlike pores. *J. Chem. Phys.* **1991**, *94*, 3183–3191.
5 Kierlik, E.; Rosinberg, M. L. Density-functional theory for inhomogeneous fluids: adsorption of binary mixtures. *Phys. Rev. A* **1991**, *44*, 5025–5037.

6 Donley, J. P.; Rajasekaran, J. J.; McCoy, J. D.; Curro, J. G. Microscopic approach to inhomogeneous polymeric liquids. *J. Chem. Phys.* **1995**, *103*, 5061–5069.
7 Yu, Y. X.; Wu, J. Z. Density functional theory for inhomogeneous mixtures of polymeric fluids. *J. Chem. Phys.* **2002**, *117*, 2368–2376.
8 Frischknecht, A. L.; Weinhold, J. D.; Salinger, A. G.; Curro, J. G.; Douglas Frink, L. J.; McCoy, J. D. Density functional theory for inhomogeneous polymer systems. I. Numerical methods. *J. Chem. Phys.* **2002**, *117*, 10385–10397.
9 Wang, Q. Correlations in hard- and soft-core generic polymer models. *Polymers* **2023**, *15*, 1180.
10 Wang, Q. Numerical analysis of PRISM-PY calculations for hard- and soft-core generic polymer models. *Chinese J. Polym. Sci.* **2024**, *42*, 1–12.
11 Evans, R.; Sluckin, T. J. A density functional theory for inhomogeneous charged fluids: Application to the surfaces of molten salts. *Mol. Phys.* **1980**, *40*, 413–435.
12 Sluckin, T. J. Applications of the density-functional theory of charged fluids. *J. Chem. Soc., Faraday Trans. 2* **1981**, *77*, 575–586.
13 Gillespie, D.; Nonner, W.; Eisenberg, R. S. Coupling Poisson Nernst Planck and density functional theory to calculate ion flux. *J. Phys. Condens. Matter* **2002**, *14*, 12129–12145.
14 Gillespie, D.; Nonner, W.; Eisenberg, R. S. Density functional theory of charged, hard-sphere fluids. *Phys. Rev. E* **2003**, *68*, 031503.
15 Roth, R.; Gillespie, D. Shells of charge: a density functional theory for charged hard spheres. *J. Phys. Condens. Matter* **2016**, *28*, 244006.
16 Roth, R.; Gillespie, D. Corrigendum: Shells of charge: a density functional theory for charged hard spheres (2016 J. Phys. Condens. Matter 28 244006). *J. Phys. Condens. Matter* **2017**, *29*, 449501.
17 Jiang, J.; Gillespie, D. Revisiting the charged shell model: a density functional theory for electrolytes. *J. Chem. Theory Comput.* **2021**, *17*, 2409–2416.
18 Wei, D.; Blum, L. Internal energy in the mean spherical approximation as compared to Debye-Hueckel theory. *J. Phys. Chem.* **1987**, *91*, 4342–4343.
19 Yu, Y. X.; Wu, J. Z. Extended test-particle method for predicting the inter- and intramolecular correlation functions of polymeric fluids. *J. Chem. Phys.* **2003**, *118*, 3835–3842.
20 Rosenfeld, Y. Free-energy model for the inhomogeneous hard-sphere fluid mixture and density-functional theory of freezing. *Phys. Rev. Lett.* **1989**, *63*, 980–983.
21 Roth, R.; Evans, R.; Lang, A.; Kahl, G. Fundamental measure theory for hard-sphere mixtures revisited: the White Bear version. *J. Phys. Condens. Matt.* **2002**, *14*, 12063–12078.
22 Yu, Y. X.; Wu, J. Z. Structures of hard-sphere fluids from a modified fundamental-measure theory. *J. Chem. Phys.* **2002**, *117*, 10156–10164.
23 Wertheim, M. S. Fluids with highly directional attractive forces. IV. Equilibrium polymerization. *J. Stat. Phys.* **1986**, *42*, 477–492.
24 Yu, Y. X.; Wu, J. Z. A fundamental-measure theory for inhomogeneous associating fluids. *J. Chem. Phys.* **2002**, *116*, 7094–7103.
25 Hansen-Goos, H.; Roth, R. Density functional theory for hard-sphere mixtures: the White Bear version mark II. *J. Phys. Condens. Matter* **2006**, *18*, 8413–25.
26 Roth, R. Fundamental measure theory for hard-sphere mixtures: a review. *J. Phys. Condens. Matter* **2010**, *22*, 063102.
27 Boublík, T. Hard-sphere equation of state. *J. Chem. Phys.* **1970**, *53*, 471–472.
28 Mansoori, G. A.; Carnahan, N. F.; Starling, K. E.; Leland, T. W. Equilibrium thermodynamic properties of the mixture of hard spheres. *J. Chem. Phys.* **1971**, *54*, 1523–1525.
29 Zmpitas, W.; Gross, J. Detailed pedagogical review and analysis of Wertheim's thermodynamic perturbation theory. *Fluid Phase Equil.* **2016**, *428*, 121–152.
30 Baxter, R. J. Ornstein-Zernike relation and Percus-Yevick approximation for fluid mixtures. *J. Chem. Phys.* **1970**, *52*, 4559–4562.
31 Blum, L. Mean spherical model for asymmetric electrolytes. *Mol. Phys.* **1975**, *30*, 1529–1535.
32 Hiroike, K. Supplement to Blum's theory for asymmetric electrolytes. *Mol. Phys.* **1977**, *33*, 1195–1198.
33 Blum, L.; Rosenfeld, Y. Relation between the free energy and the direct correlation function in the mean spherical approximation. *J. Stat. Phys.* **1991**, *63*, 1177–1190.
34 Blum, L.; Hoeye, J. S. Mean spherical model for asymmetric electrolytes. 2. Thermodynamic properties and the pair correlation function. *J. Phys. Chem.* **1977**, *81*, 1311–1316.
35 Lebowitz, J. L. Exact solution of generalized Percus-Yevick equation for a mixture of hard spheres. *Phys. Rev.* **1964**, *133*, A895–A899.
36 Hiroike, K. Ornstein-Zernike relation for a fluid mixture with direct correlation functions of finite range. *J. Phys. Soc. Japan* **1969**, *27*, 1415–1421.
37 Rosenfeld, Y. Free energy model for inhomogeneous fluid mixtures: Yukawa-charged hard spheres, general interactions, and plasmas. *J. Chem. Phys.* **1993**, *98*, 8126–8148.
38 Boda, D.; Fawcett, W. R.; Henderson, D.; Sokołowski, S. Monte Carlo, density functional theory, and Poisson-Boltzmann theory study of the structure of an electrolyte near an electrode. *J. Chem. Phys.* **2002**, *116*, 7170–7176.
39 Valiskó, M.; Kristóf, T.; Gillespie, D.; Boda, D. A systematic Monte Carlo simulation study of the primitive model planar electrical double layer over an extended range of concentrations, electrode charges, cation diameters and valences. *AIP Adv.* **2018**, *8*, 025320.
40 Voukadinova, A.; Valisko, M.; Gillespie, D. Assessing the accuracy of three classical density functional theories of the electrical double layer. *Phys. Rev. E* **2018**, *98*, 012116.
41 Jiang, J.; Ginzburg, V. V.; Wang, Z. G. Density functional theory for charged fluids. *Soft Matter* **2018**, *14*, 5878–5887.
42 Jiang, J.; Ginzburg, V. V.; Wang, Z. G. On the origin of oscillatory interactions between surfaces mediated by polyelectrolyte solution. *J. Chem. Phys.* **2019**, *151*, 214901.
43 Gillespie, D.; Valiskó, M.; Boda, D. Density functional theory of the electrical double layer: the RFD functional. *J. Phys. Condens. Matter* **2005**, *17*, 6609–6626.
44 Andersen, H. C.; Chandler, D. Optimized cluster expansions for classical fluids. I. General theory and variational formulation of the mean spherical model and hard sphere Percus-Yevick equations. *J. Chem. Phys.* **1972**, *57*, 1918–1929.
45 Li, Z. D.; Wu, J. Z. Density functional theory for polyelectrolytes near oppositely charged surfaces. *Phys. Rev. Lett.* **2006**, *96*, 048302.
46 Li, Z. D.; Wu, J. Z. Density functional theory for planar electric double layers: closing the gap between simple and polyelectrolytes. *J. Phys. Chem. B* **2006**, *110*, 7473–7484.
47 Patra, C. N.; Chang, R.; Yethiraj, A. Structure of polyelectrolyte solutions at a charged surface. *J. Phys. Chem. B* **2004**, *108*, 9126–9132.
48 Jiang, T.; Wu, J. Self-organization of multivalent counterions in polyelectrolyte brushes. *J. Chem. Phys.* **2008**, *129*, 084903.
49 Chang, Q.; Jiang, J. Sequence effects on the salt-enhancement behavior of polyelectrolytes adsorption. *Macromolecules* **2022**, *55*, 897–905.
50 Qing, L.; Jiang, J. Enabling high-capacitance supercapacitors by

polyelectrolyte brushes. *ACS Nano* **2023**, *17*, 17122–17130.
51 Jiang, T.; Li, Z.; Wu, J. Structure and swelling of grafted polyelectrolytes: predictions from a nonlocal density functional theory. *Macromolecules* **2006**, *40*, 334–343.
52 Jiang, T.; Wu, J. Ionic effects in collapse of polyelectrolyte brushes. *J. Phys. Chem. B* **2008**, *112*, 7713–7720.
53 Wang, L.; Liang, H.; Wu, J. Electrostatic origins of polyelectrolyte adsorption: theory and Monte Carlo simulations. *J. Chem. Phys.* **2010**, *133*, 044906.
54 Li, Z.; Wu, J.; Wang, Z. G. Osmotic pressure and packaging structure of caged DNA. *Biophys. J.* **2008**, *94*, 737–746.
55 Jiang, T.; Wang, Z. G.; Wu, J. Electrostatic regulation of genome packaging in human hepatitis B virus. *Biophys. J.* **2009**, *96*, 3065–3073.
56 Meng, D.; Hjelm, R. P.; Hu, J.; Wu, J. A theoretical model for the dynamic structure of hepatitis B nucleocapsid. *Biophys. J.* **2011**, *101*, 2476–2484.
57 Cheng, J.; Xu, J.; Yang, J.; Lv, W.; Lian, C.; Liu, H. Enhanced oil recovery by sacrificing polyelectrolyte to reduce surfactant adsorption: a classical density functional theory study. *Chem. Eng. Sci.* **2022**, *261*, 117957.
58 Balzer, C.; Jiang, J.; Marson, R. L.; Ginzburg, V. V.; Wang, Z. G. Nonelectrostatic adsorption of polyelectrolytes and mediated interactions between solid surfaces. *Langmuir* **2021**, *37*, 5483–5493.
59 Chang, Q.; Jiang, J. Force regulation by sequence-defined polyelectrolytes. *Macromolecules* **2023**, *56*, 4100–4110.
60 Chang, Q.; Jiang, J. Nanoscale hierarchical structures formed by sequence-defined polycations and homopolyanions for high salt-tolerance adhesives. *Macromolecules* **2024**, *57*, 1859–1867.
61 Qing, L.; Jiang, J. Interfacial microstructure of neutral and charged polymer brushes: a density functional theory study. *J. Chem. Phys.* **2022**, *157*, 224904.
62 Prusty, D.; Gallegos, A.; Wu, J. Unveiling the role of electrostatic forces on attraction between opposing polyelectrolyte brushes. *Langmuir* **2024**, *40*, 2064–2078.
63 Brown, J. R.; Seo, Y.; Maula, T. A.; Hall, L. M. Fluids density functional theory and initializing molecular dynamics simulations of block copolymers. *J. Chem. Phys.* **2016**, *144*, 124904.
64 Frischknecht, A. L.; Curro, J. G.; Douglas Frink, L. J. Density functional theory for inhomogeneous polymer systems. II. Application to block copolymer thin films. *J. Chem. Phys.* **2002**, *117*, 10398–10411.
65 Liu, Y.; Liu, H. Development of 3D polymer DFT and its application to molecular transport through a surfactant-covered interface. *AIChE J.* **2017**, *64*, 238–249.
66 Matsen, M. W. Fast and accurate SCFT calculations for periodic block-copolymer morphologies using the spectral method with Anderson mixing. *Eur. Phys. J. E* **2009**, *30*, 361–369.
67 Arora, A.; Morse, D. C.; Bates, F. S.; Dorfman, K. D. Accelerating self-consistent field theory of block polymers in a variable unit cell. *J. Chem. Phys.* **2017**, *146*, 244902.
68 Qiang, Y.; Li, W. Accelerated pseudo-spectral method of self-consistent field theory via crystallographic fast Fourier transform. *Macromolecules* **2020**, *53*, 9943–9952.
69 Chang, R.; Yethiraj, A. Osmotic pressure of salt-free polyelectrolyte solutions: a Monte Carlo Simulation study. *Macromolecules* **2004**, *38*, 607–616.
70 Bizjak, A.; Rescic, J.; Kalyuzhnyi, Y. V.; Vlachy, V. Theoretical aspects and computer simulations of flexible charged oligomers in salt-free solutions. *J. Chem. Phys.* **2006**, *125*, 214907.
71 Ni, R.; Cao, D.; Wang, W. A Monte Carlo study of spherical electrical double layer of macroions-polyelectrolytes systems in salt free solutions. *J. Phys. Chem. B* **2006**, *110*, 26232–26239.
72 Sajevic, T.; Reščič, J.; Vlachy, V. Correlation between flexibility of chain-like polyelectrolyte and thermodynamic properties of its solution. *Condens. Matter Phys*. **2011**, *14*, 33603.
73 Jiang, H.; Adidharma, H. Monte Carlo simulation and equation of state for flexible charged hard-sphere chain fluids: polyampholyte and polyelectrolyte solutions. *J. Chem. Phys.* **2014**, *141*, 174906.
74 Chang, R.; Kim, Y.; Yethiraj, A. Osmotic pressure of polyelectrolyte solutions with salt: grand canonical Monte Carlo simulation studies. *Macromolecules* **2015**, *48*, 7370–7377.
75 Chandler, D.; McCoy, J. D.; Singer, S. J. Density functional theory of nonuniform polyatomic systems. I. General formulation. *J. Chem. Phys.* **1986**, *85*, 5971–5976.
76 Chandler, D.; McCoy, J. D.; Singer, S. J. Density functional theory of nonuniform polyatomic systems. II. Rational closures for integral equations. *J. Chem. Phys.* **1986**, *85*, 5977–5982.
77 Hooper, J. B.; McCoy, J. D.; Curro, J. G. Density functional theory of simple polymers in a slit pore. I. Theory and efficient algorithm. *J. Chem. Phys.* **2000**, *112*, 3090–3093.
78 Sen, S.; McCoy, J. D.; Nath, S. K.; Donley, J. P.; Curro, J. G. The structure of a rotational isomeric state alkane melt near a hard wall: comparison of density functional theory with related theories. *J. Chem. Phys.* **1995**, *102*, 3431–3439.
79 Cao, D.; Jiang, T.; Wu, J. A hybrid method for predicting the microstructure of polymers with complex architecture: combination of single-chain simulation with density functional theory. *J. Chem. Phys.* **2006**, *124*, 164904.